GLOBAL BIOGEOCHEMICAL CYCLES, VOL. 10, NO. 4, PAGES 559-583, DECEMBER 1996

Effects of plankton dynamics on seasonal carbon fluxes in an ocean general circulation model

Katharina D. Six and Ernst Maier-Reimer
Max-Planck-Institut für Meteorologie, Hamburg, Germany

Abstract. We discuss the effect of embedding a simple plankton model in the Hamburg model of the oceanic carbon cycle (HAMOCC3) [*Maier-Reimer*, 1993]. The plankton model consists of five components: phytoplankton, zooplankton, detritus, dissolved organic carbon, and nutrients. Interactions between compartments are described by one global set of parameters. Despite its simplicity the plankton model reproduces regional differences in seasonal oceanic pCO_2 and improves the biogeochemical tracer distributions at the depth of the oxygen minimum in the Pacific Ocean. The predicted seasonal turnover of organic material is consistent with recent atmospheric O_2 measurements in the remote areas of the Southern Ocean.

1. Introduction

The geochemical state of the ocean results to some degree from biological processes. A complete switch-off of photosynthesis would produce substantial change in this chemical state, and also in atmospheric pCO_2, within a very few years. In studies of the oceanic uptake of CO_2 from fossil fuels, biological activity within the ocean has been thought not to be an important process [*Maier-Reimer and Hasselmann*, 1987; *Sarmiento et al.*, 1992; *Broecker*, 1991; *Maier-Reimer et al.*, 1996]. The basic state of abiotic three-dimensional (3-D) circulation models, however, could not be compared with distributions in the real ocean because marine biological activity is responsible for 80% of the observed vertical gradient of dissolved inorganic carbon (ΣCO_2).

First attempts to include the impact of the biological pump on the carbon distributions in global 3-D circulation models were made by *Bacastow and Maier-Reimer* [1990], *Najjar et al.* [1992], and *Maier-Reimer* [1993]. To estimate the flux of particulate organic material (POM) into the ocean interior, *Najjar et al.* [1992] used a restoring technique in which predicted surface phosphate concentration is adjusted toward observed surface phosphate concentration. *Bacastow and Maier-Reimer* [1990] used phosphate based Michaelis-Menten kinematics, modified by a light factor, to predict the flux of POM. Remineralization of POM at depth results in a concentration increase of inorganic phosphate and a concentration decrease in oxygen. Both Bacastow and Maier-Reimer and Najjar et al. predict unrealistically high phosphate accumulation in the equatorial region. This "nutrient trapping" led to the conclusion that a considerable amount of the new production flux to the ocean interior must be carried by dissolved organic matter (DOM). If DOM has a "lifetime" of a few years, or even decades, advection of the DOM would carry nutrients away from the regions of strong upwelling and thereby avoid nutrient trapping. Najjar et al. achieved a good simulation of the deep PO_4 distribution by assuming a DOM lifetime of more than 100 years. However, their approach strongly relies on the quality of wind stress data, which determine the upwelling, and the quality of surface phosphate data. These are questionable, especially in the Southern Ocean, where Najjar et al.'s approach predicts an extremely high new production (twice the equatorial value).

Maier-Reimer [1993] parameterized the annual net effect of biological processes on surface tracers in the Hamburg model of the oceanic carbon cycle (HAMOCC3) by one globally uniform uptake rate for phosphate (0.25 month^{-1}, modified locally by temperature, solar angle, and vertical stirring rates). He chose this time constant in order to achieve observed annual mean large-scale gradients between surface and deeper water phosphate. The phosphate uptake, modified by appropriate transfer functions, provides the basis for predicting changes of all tracers involved in the marine biology (i.e., ΣCO_2, alkalinity, oxygen, and silicate). The surface tracer change is equal to the production of particulate organic material (POM) and of shell material. Shells and POM are transported, according to assumed distribution functions, to greater depth, where remineralization of POM and dissolution of shells lead to a change in tracer concentrations. The model repro-

Paper number 96GB02561.
0886-6236/96/96GB-02561$12.00

duced the observed large-scale vertical tracer gradients, but there still remained the problem of nutrient trapping in the Equatorial Pacific. Also, comparisons with observed seasonal variations of surface properties, for example, pCO_2, revealed that this biological production scheme is not suitable for reproducing this aspect of the measurements. In particular, in regions where biological production leads to pronounced pCO_2 variation, for example, in the North Atlantic [*Watson et al.*, 1991], it produces an insufficient seasonal amplitude and a phase shift between observations and simulations.

A better agreement between the simulated and observed seasonal amplitude of pCO_2 can be achieved by enhancing the phosphate uptake rate in HAMOCC3 (Figure 1a). This is consistent with the fact that a nearly complete nutrient depletion may occur in spring within a very short period of time [*Takahashi et al.*, 1993]. However, a higher phosphate uptake rate leads to an almost complete depletion of phosphate in the surface waters of the subtropical gyres (Figure 1b). The circulation field brings only a limited amount of phosphate to the surface layer. The enhanced incorporation of phosphate into POM and its export from the surface layer in upwelling areas result in a strong PO_4 depletion in surface areas that are only supported by lateral PO_4 advection, as in the subtropical gyres. In addition to the still inferior surface phosphate distribution the approach with an increased uptake rate intensifies nutrient trapping in the Pacific [*Maier-Reimer and Bacastow*, 1990]. On the basis of these considerations we conclude that a first-order process is missing in the geochemical, or more specifically, in that simple biological part of the model.

In this paper we discuss the effects of a simple plankton model on tracer distributions as simulated with HAMOCC3. The extended model is henceforth referred

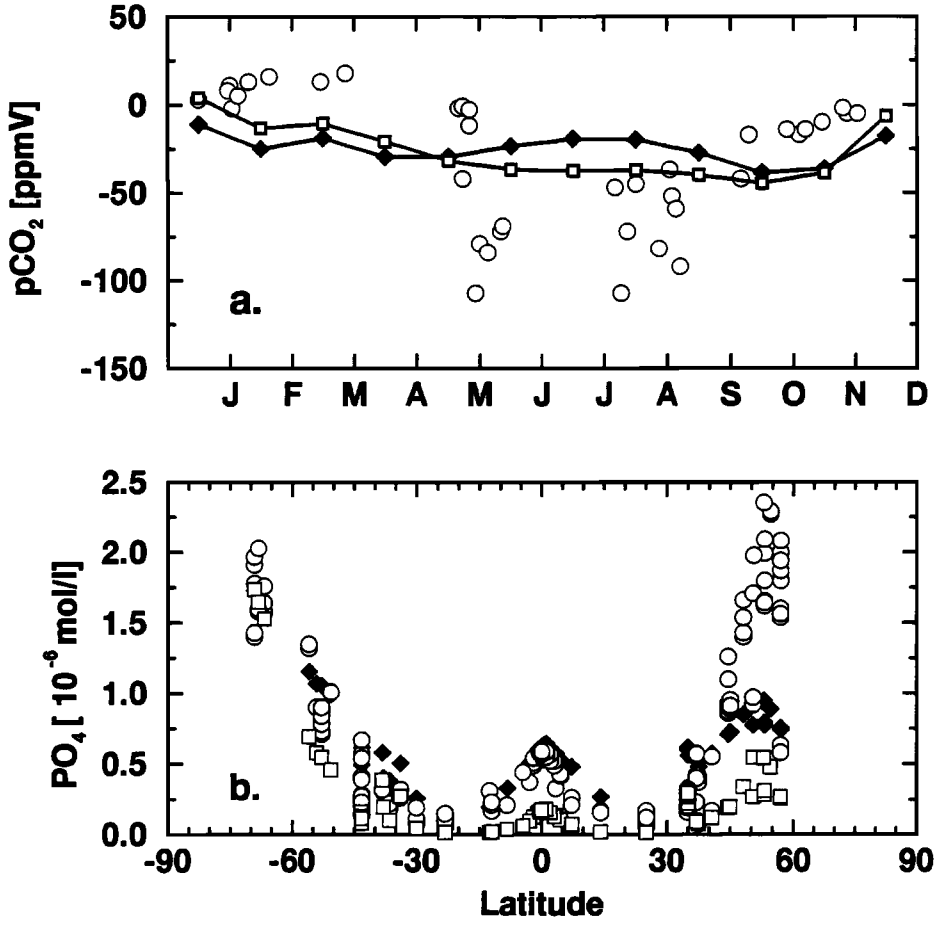

Figure 1. (a) Seasonal variation of ΔpCO_2 from observations at Iceland (64°N 25°W; years, 1983-1985 [*Takahashi et al.*, 1993]) (open circles) and simulations with HAMOCC3 for two different PO_4 uptake rates (solid diamonds, standard version $r_0 = 0.25$ month^{-1} [*Maier-Reimer*, 1993] and open squares, high $r_0 = 1.0$ month^{-1}) (b) Meridional PO_4 concentration along 180° from observations [*Conkright et al.*, 1994]. Simulated concentrations taken from model results at the same locations and times as observations are shown. Symbol notation is the same as in Figure 1a.

to as HAMOCC3.1. The goal is to achieve a dynamically consistent field of seasonal oceanic pCO_2. We are able to simulate variations of surface pCO_2, as observed at various locations, with a plankton model of a most simple structure. It consists of only five compartments: nutrients, phytoplankton, grazers, detritus, and dissolved organic carbon (DOC). Their interactions are described by a minimal set of tunable parameters. The seasonal growth of phytoplankton leads to a drawdown of surface pCO_2. The occurrence of blooms, which result in abrupt reductions of surface pCO_2, is thought to be mainly caused by variation in the abundance of grazers [*Evans and Parslow*, 1985; *Frost*, 1991]. Thus, to address regional differences in pCO_2 variations, we include grazing pressure by zooplankton. Sensitivity studies showed that we need to include the production of DOC if we want to simulated both observed variations of pCO_2 and realistic phytoplankton concentrations.

The presented paper describes the structure of the plankton model and discusses the simulations of the oceanic pCO_2. Comparison with globally observed distributions of phosphate and chlorophyll allow us to deduct the quality of our results. In addition, the variations of the sea-to-air oxygen flux provide independent information to test the biological part of the model in the remote area of the Southern Ocean and to give us some confidence in our model approach.

2. Model

The HAMOCC3 is a global marine carbon cycle model with a horizontal resolution of 3.5 by 3.5 degrees and realistic topography. The vertical direction is resolved by 15 layers with a higher resolution in the upper water column (depth levels at 50, 100, 150, 200, 250, 300, 400, 525, 700, 900, 1500, 2500, 3500, 4500, and 6000 m). Distributions of various biochemical tracers involved in the carbon system are simulated on the basis of the circulation field from an ocean general circulation model. The large-scale geostrophic circulation model (LSG) [*Maier-Reimer et al.*, 1993], provides velocity, temperature, and salinity fields, so that transport, chemical reactions, and gas exchange across the air-sea interface can be determined for components of the carbon system. The circulation model and carbon cycle model operate with the same 1-month time step. Temperature, salinity, velocity field, and convective events are taken from the last year of a 5000-year integration of the circulation model.

The circulation model provides the basic information that is necessary for the construction of a global tracer model [*Maier-Reimer*, 1993]. The change in tracer concentration is given by advection as well as by local sources and sinks. In the carbon cycle one local sink (source) is the marine biota, where dissolved inorganic carbon is stored in (released from) organic material and calcite shells. The parameterization of the effects of marine biology on ΣCO_2 and thus pCO_2 is the central concern of this paper.

Another source/sink is gas exchange, which occurs only at the sea surface. Gas exchange is determined by the product of the local air-sea partial pressure difference of CO_2 and a gas exchange coefficient. The spatial and temporal distribution of the gas exchange coefficient was derived by *Heimann and Monfray* [1989] from an empirical function of *Liss and Merlivat* [1986] that relates the exchange coefficient to the wind speed. Instead of using only the average wind speed, *Heimann and Monfray* [1989] based their calculations also on a wind speed statistic to allow for the nonlinear characteristic of the gas exchange coefficient at high wind speeds. The gas exchange coefficient matrix is normalized to a global average of 0.06 mol (ppm yr $m^2)^{-1}$ to match the global estimate from radiocarbon studies [*Broecker et al.*, 1985]. The necessary chemical constants to determine pCO_2 from the concentrations of alkalinity and dissolved inorganic carbon in sea water are taken from *Weiss* [1974], *Goyet and Poisson* [1989], and *Edmond and Gieskes* [1970]. The model inventories of alkalinity and ΣCO_2 were tuned to achieve a preindustrial atmospheric pCO_2 level of 278 parts per million by volume. For mass balance reasons we include an atmospheric box, which is completely mixed in the zonal direction within 1 month. Along meridians a diffusive mixing is prescribed with an interhemispheric exchange time of about 1.3 years.

In HAMOCC3 a first-order approach is taken to simulating the biologically induced carbon flux from the surface toward the interior of the ocean. A biological production term is estimated from a single time constant for the uptake of surface phosphate (PO_4) [*Maier-Reimer*, 1993]. Except for the East Equatorial Pacific (see below) this approach is sufficient for simulating the vertical tracer gradient. However, the predicted annual pCO_2 cycle is then globally dominated by the temperature dependent solubility effect. Recently, several pCO_2 time series have become available [*Takahashi et al.*, 1993; *Wong and Chan*, 1991] showing a strong impact from biological processes on the seasonal pCO_2 variation. The resulting behavior is quite different from the temperature dependent solubility effect. As stated above, we do not see any possibility to simulate the pCO_2 seasonality and the gradient of surface phosphate with only one time constant for nutrient depletion and export production. Thus a more sophisticated biological production scheme must be considered.

We base our biological production scheme on five compartments (Figure 2): phosphate (N), as limiting nutrient, phytoplankton (P), zooplankton (Z), particulate organic carbon (POC), and dissolved organic carbon (DOC). POC is considered to be only "dead" or-

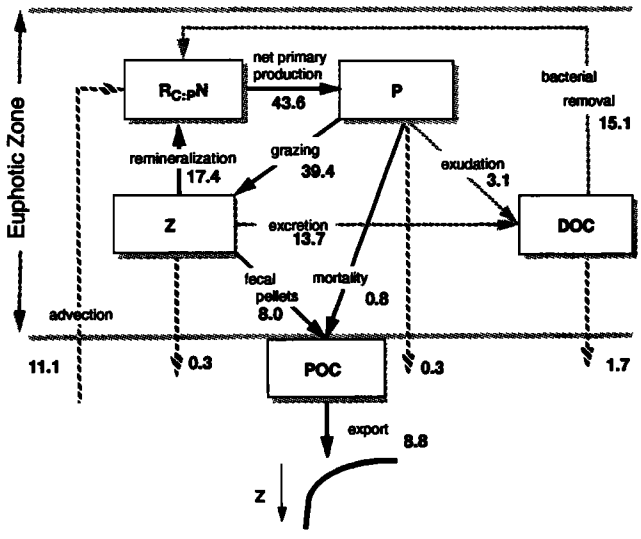

Figure 2. Schematic diagram of the processes simulated by HAMOCC3.1. Carbon fluxes between different compartments of the HAMOCC3.1 are given in Gt C yr^{-1}.

ganic carbon, that is, phytodetritus and fecal pellets from herbivores and carnivores as well as suspended organic carbon. POC produced in the surface layer is exported immediately to deeper layers according to a power law distribution function [*Suess*, 1980]. The divergence of the Suess function equals the disaggregation of large particles and is therefore a source of neutrally buoyant suspended organic carbon that is then subject to remineralization. DOC is exudated by phytoplankton and zooplankton at a constant rate and remineralized according to a chosen decay time. DOC is not affected by gravitational sinking. It can only be subducted by the ocean currents. Thus the DOC pool acts as an additional organic carbon pool that is not photosynthetically active but stores carbon temporarily in an organic form within the euphotic layer. A certain amount of inorganic carbon has to be incorporated into organic material to achieve a reasonable seasonal cycle of surface pCO_2. Earlier experiments [*Kurz*, 1993] have shown that we are able to simulate acceptable oceanic pCO_2 values only in the vicinity of unrealistically high concentrations of phytoplankton (a factor 2-5 higher than observed). On the other hand, recent measurements in the North Atlantic have revealed a distinct seasonal cycle in surface DOC with variations of 40 μmol C L^{-1} between winter and summer [*Bodungen and Kähler*, 1994]. Thus we included this labile fraction of DOC, with a decay rate of less than 1 year, in our simulation. The refractory background concentration of DOC ($\approx$ 40 μmol C L^{-1}, [*Murray et al.*, 1994]) does not contribute to the seasonal variation and is therefore not considered.

Apart from the effects of advection and gas exchange, the monthly change in the inorganic carbon concentration in surface waters is caused by the net production (or decay) of biomass. Thus we specify that nutrient and CO_2 uptake results immediately in biomass increase. Photosynthetic processes in phytoplankton and the life history of zooplankton are not considered. Changes of and interaction between the various compartments of HAMOCC3.1 are given by the following equations (see Figure 2 also). For completeness we include the abbreviation $\mathcal{AD}(\ )$. It denotes the concentration change only due to hydrodynamical processes, that is, advection, vertical convection, and diffusion.

nutrient change

$$\begin{aligned} R_{C:P}\frac{\partial N}{\partial t} &= \mathcal{AD}(N) - r(T,L)\frac{N}{N+N_0}P \\ &\quad + g(T)\epsilon_{her}(1-\text{zinges})\frac{(P-P_{min})}{P+P_0}Z \\ &\quad + \epsilon_{can}\, d_z(Z-Z_{min}) \\ &\quad + r_{doc}(N)DOC + l(O_2) \end{aligned}$$

where the second term on the right hand side denotes phytoplankton growth, the third term denotes remineralization from herbivores, the fourth term denotes remineralization from carnivores, the fifth term denotes decay of DOC, and $l(O_2)$ denotes remineralization of POC (only for z > 100 m).

phytoplankton change

$$\begin{aligned} \frac{\partial P}{\partial t} &= \mathcal{AD}(P) + r(T,L)\frac{N}{N+N_0}P \\ &\quad - g(T)\frac{(P-P_{min})}{P+P_0}Z - d_p(P-P_{min}) \\ &\quad - \gamma_P(P-P_{min}) \end{aligned}$$

where the second term denotes phytoplankton growth, the third term denotes grazing loss from herbivores, the fourth term denotes natural senescence, and the fifth term denotes exudation of DOC.

zooplankton change

$$\begin{aligned} \frac{\partial Z}{\partial t} &= \mathcal{AD}(Z) + g(T)\epsilon_{her}\,\text{zinges}\,\frac{(P-P_{min})}{P+P_0}Z \\ &\quad - d_z(Z-Z_{min}) - \gamma_Z(Z-Z_{min}) \end{aligned}$$

where the second term denotes growth from grazing,

the third term denotes loss from grazing by carnivores, and the fourth term denotes excretion of DOC.

DOC change

$$\frac{\partial DOC}{\partial t} = \mathcal{AD}(DOC) + \gamma_P(P - P_{\min}) + \gamma_Z(Z - Z_{\min}) - r_{\text{doc}}(N)DOC$$

where the second term denotes DOC exudation from phytoplankton, the third term denotes DOC excretion from zooplankton, and the fourth term denotes decay of DOC.

POC change

$$\frac{\partial POC}{\partial t} = \mathcal{AD}(POC) + F(d_p, d_z, \epsilon_{\text{her}}, \epsilon_{\text{can}}, P, Z, z) - l(O_2)$$

with $l(O_2)$ denotes the remineralization of POC (only for z > 100 m) and

$$F(d_p, d_z, \epsilon_{\text{her}}, \epsilon_{\text{can}}, P, Z, z) = 0$$

for $0 < z < 100$ m and otherwise

$$F(d_p, d_z, \epsilon_{\text{her}}, \epsilon_{\text{can}}, P, Z, z) = \text{TPP}\,\frac{\partial}{\partial z}\left(\frac{z}{100\text{ m}}\right)^{-0.8}$$

$F(\,)$ describes the flux of "dead" organic carbon to the ocean interior. All particles that stem from natural senescence or fecal pellet production within the euphotic layer are summarized in the total particle production per month:

$$\text{TPP} = \int_0^{100\text{ m}} (g(T)(1 - \text{zinges})(1 - \epsilon_{\text{her}}) \frac{(P - P_{\min})}{P + P_0} Z + d_p(P - P_{\min}) + d_z(1 - \epsilon_{\text{can}})(Z - Z_{\min}))$$

Particles leave the euphotic layer (i.e., no POC source for $z < 100$ m), are distributed according to the particle flux function of *Suess* [1980], and decay if there is enough oxygen available (see below).

It is widely assumed that in pelagic seas the availability of nitrate governs biological production. However, it has been observed that biological production, that is, carbon fixation, continues even at extremely low nitrate levels [*Banse*, 1994]. Other forms of nitrogen, for example, ammonium and urea, which are recycled products from zooplankton and other higher trophic levels, and nitrogen pools within cells can maintain this production [*Dugdale and Goering*, 1967]. For a description of this complex nitrogen cycling one would have to consider a number of additional, not well-understood processes. However, the utilization of nitrogen is accompanied by phosphate uptake, and to first order the stoichiometric phosphorus to nitrogen ratio (in moles) within the ocean is almost perfectly constant [*Redfield et al.*, 1963; *Takahashi et al.*,1985]. Only in extreme oligotrophic regions does nitrate appear to be more strongly depleted than phosphate [*Bainbridge*, 1980, 1981]. If we accept the temporal and regional constancy of Redfield ratios, we can relate biological production to phosphate concentration. The resulting phosphate distribution is then directly comparable to global PO_4 observations [*Conkright et al.*, 1994].

The maximum phytoplankton growth rate per day, $r(T, L)$, is a function of temperature and total incoming light. Various mathematical formulations describing the relationship between plant growth and light were compared by *Jassby and Platt* [1976]. They found that a good fit to observations is given by the formula of *Smith* [1936]:

$$r(T, L) = \frac{f(T) \cdot f(L)}{\sqrt{(f(T)^2 + f(L)^2)}} \quad (1)$$

All relationships that were compared describe the primary productivity by only three parameters: local irradiance, the slope of the light saturation curve at low light levels α, and the specific growth rate at optimal illumination. The latter is a function of temperature $f(T)$, given by a formula of *Eppley* [1972]:

$$f(T) = a \cdot b^{cT} \quad (2)$$

where the coefficients a, b, and c are taken from Eppley (see Table 1) and T is temperature in degree Celsius. The light dependency is given by

$$f(L) = I_0 \cdot \alpha \cdot \text{PAR} \cdot \frac{1}{z} \cdot \int_z e^{-k \cdot z} dz \quad (3)$$

Of the incoming light I_0 only the portion of photosynthetically active radiation PAR is available for photosynthesis. Values for α and PAR and their units are listed in Table 1. The regional and seasonal distribution of I_0 is taken from 8 years of daily 12-hour weather analyses from the European Centre for Medium-Range Weather Forcasts (ECMWF). We have calculated a monthly mean field of I_0 from all available ECMWF data of the corresponding month for that grid box. Variations of the diurnal cycle are included in these data. Biological production is suppressed under the sea ice cover predicted by the LSG.

Light penetration decreases with depth according to an exponential function with an extinction factor k. In

(3) we have calculated the mean solar radiation which can be harvested by plankton by integrating the light function over each depth level. Owing to the coarse vertical resolution we get only mean plankton concentration for each productive layer. Therefore we did not include self shading.

Variations in the mixed layer depth have a strong impact on the development of plankton blooms [*Sverdrup*, 1953]. As long as the mixed layer extends down to a depth greater than light can penetrate, as it does in early spring, plankton spends time out of the euphotic zone. Thus mean growth is reduced relative to growth with a shallower mixed layer. With stabilization of the water column later in the spring the mixing depth shoals and the mean light yield increases. It is generally believed that the timing of plankton blooms is mainly controlled by the development of a shallow mixed layer. The vertical resolution of our model is 50 m in the upper 300 m of the water column. There is no explicit mixed layer formulation; that is, the wind energy input from the atmosphere is limited to the uppermost model layer. To get the necessary information for (3), we diagnosed a mixed layer depth z_m on the basis of the simulated density gradient and the prescribed wind stirring.

At the ocean surface ($z = z_m \rightarrow 0$), $r(T, L)$ reaches values between 0 and 2.5 d^{-1}, depending on the temperature and irradiance. Phytoplankton growth is restricted to the upper 100 m (first two layers in the model). If the predicted mixed layer depth z_m is deeper than 75 m, the specific growth rate $r(T, L)$ is identical in both layers with

$$r_{\text{layer1}} = r_{\text{layer2}} = 1/z_m \cdot \int_0^{z_m} r(T, L)$$

If the mixed layer depth is shallower than 75 m

$$r_{\text{layer1}} = 1/z_m \cdot \int_0^{z_m} r(T, L)$$

$$r_{\text{layer2}} = 1/\Delta z_2 \cdot \int_{\Delta z_2} r(T, L)$$

where Δz_2 represents the depth interval from 50 to 100 m.

The specific growth rate of phytoplankton determined for the first layer always depends on the predicted mixed layer depth even if z_m is shallower than 50 m. The coarse vertical resolution and thus the limited possibility to separate the euphotic zone in different production regions (e.g., above the mixed layer depth with good specific growth rate and usually low nutrients content) might result in an overestimate of the depth-integrated net primary production. However, neither net primary production nor specific growth rates are known exactly on the global scale. Therefore we have to deduct the quality of our results from the effects that our choice of parameters has on global geochemical tracer distribution. A finer vertical resolution of the model would, certainly, be advantageous for the simulation of biological processes. However, in view of the intended future application of this model configuration for climate studies we have to consider restricted computing time and memory resources.

Nutrient availability is described by Michaelis-Menten kinetics with a half-saturation constant N_0. The value of N_0 was chosen to be 0.016 μmol P L^{-1}, which is within the range of open ocean values given by *Eppley et al.* [1969], when transformed to nitrogen units by the Redfield ratio.

Phytoplankton concentration is diminished by zooplankton activity, natural senescence, and exudation of dissolved organic carbon. The latter two are described by linear functions of phytoplankton concentration. We assume a Michaelis-Menten type function for zooplankton grazing since food supply becomes more difficult when only a few phytoplankton cells are available [*Lampert and Sommer*, 1993]. To prevent extinction of plankton, we prescribe a minimum concentration for phytoplankton and zooplankton, $P_{\min}$ and $Z_{\min}$, respectively. The constraint of a minimum concentration is necessary to maintain a biologically active ocean, but it can also be justified by the fact that the model is not designed to simulate the different reproductive and developmental stages of plankton.

Grazing by zooplankton is given by (see Table 1 for units)

$$g(T) = g_0 \cdot 1.01^{cT} \tag{4}$$

Since both the filtering rate and the respiration rate, which are acting opposite in sign on the net growth, increase with increasing temperature, we assume only a relatively small variation of g with temperature (a Q_{10} of about 1.10). Not much is known about how temperature influences the net growth of zooplankton. Higher filtering rates as well as higher respiration rates have been observed with increasing temperature [*Parsons et al.*, 1984, and references therein]. In similar simulations, *Frost* [1987] used a Q_{10}=2 dependency of grazing at Station P in the Pacific, while *Sarmiento et al.* [1993] prescribed a temperature independent grazing rate for their North Atlantic study. With our weak temperature dependency the basic grazing rate increases by about one fourth from polar waters to the tropical region. Thus tropical grazers have a slightly faster response to changes in the phytoplankton population, which can be justified by the observation of faster reproduction cycles of tropical species [see, e.g., *Raymont*, 1983].

Only a part of the ingested food leads to a biomass increase of zooplankton ($\epsilon_{\text{her}} \cdot$ zinges). The remainder is either stored in fecal pellets or metabolized, that is, remineralized to or respired as inorganic components. Fecal pellet production is assumed to be $(1 - \epsilon_{\text{her}})$ of

the ingested food. The fraction of food that is instantaneously decomposed in the surface water is given by $\epsilon_{her} \cdot (1 - \text{zinges})$. These remineralized nutrients are immediately available for phytoplankton production.

Like phytoplankton, zooplankton concentration is affected by grazing activities of higher trophic levels. Since we do not simulate the whole food chain, we assume that zooplankton dies at a constant rate d_z. The major part of this organic carbon is instantaneously remineralized (ϵ_{can}). The remaining fraction is considered to be fecal pellets and exported out of the euphotic layer.

Remineralization products within the surface layer stem additionally from the decay of dissolved organic carbon. Bacteria live in the upper water column and consume DOC at high rates. *Kirchman et al.* [1991] find DOC degradation rates of 0.025 per day with an incubation method. With such high turnover rates, DOC concentration decreases rapidly with increasing depth. Global mean downward advection of DOC halves from 3.6 Gt C yr^{-1} to 1.7 Gt C yr^{-1} between 50 m and 100 m. In 300-m water depth the model predicts a global mean DOC concentration that is only 1% of the surface value. This is consistent with observations in the Sargasso Sea where seasonal DOC variations are seen mainly in the upper 100 m [*Carlson et al.*, 1994]. To be able to metabolize DOC, bacteria also need nutrients. In a recent study, *Amon and Benner* [1994] postulate that the availability of nutrients regulates the bacterial consumption of DOC. Accordingly, we describe the decay by a saturation function:

$$r_{doc}(N) = d_0 \cdot \frac{N}{N + k_d} \tag{5}$$

In oligotrophic areas with phosphate concentrations less than 0.1 μmol P L^{-1}, the nutrient dependency reduces the decay to 10% of the base rate d_0. As stated above, the modification of the basic degradation rate gives credit mainly to the horizontal pattern of bacterial activity. The model predicts a constant DOC pool of about 8 Gt C.

Fecal pellets do not stay in the surface water. It has been observed that they sink with the remarkable speed of about 100 m per day to greater depth [*Degens et al.*, 1984]. We consider fecal pellets and carbon from natural senescence (combined as TPP) to be exported immediately after production. TPP is distributed over depth according to the power law function of *Suess* [1980] and added to the local POC concentration. All carbon stored in fecal pellets that reaches the seafloor accumulates in a sediment layer and is subsequently subject to remineralization. The global predicted sediment pool of organic carbon is 5.4 Gt C.
The Suess function describes the divergence of the vertical flux of organic matter. However, no discrimination is possible between remineralization and just mechanical disaggregation. The latter results in suspended matter, where carbon is still fixed in organic from. We allow POC to be remineralized at a constant rate l_0 while consuming oxygen according to the Redfield ratio $R_{C:O_2} = 122$:-172 (by moles). Since we do not simulate denitrification processes, we have to restrict remineralization to areas with enough oxygen. Thus remineralization of POC occurs according to

$$l(O_2) = \max(l_0 \cdot POC, R_{C:O_2} \cdot O_2) \tag{6}$$

In this way we maintain a strictly Redfield ocean, but POC accumulates in regions of low oxygen where in the real ocean, denitrification allows a continuation of POC decay. Also, inconsistencies between the biological and dynamical model will be reflected in the POC distribution (see section 3.4).

All parameters and their values are listed in Table 1. As far as possible, values are taken from the literature. Other values (e.g., the decay rate of DOC) are chosen in accordance with other model studies [e.g., *Fasham et al.*, 1993] and modified to achieve consistency with available measurements. The details of parameter choice will be the subject of further investigations. We emphasize, however, that not all details of the parametrization are of major importance for the global distribution of measurable quantities.

The biological surface processes are characterized by rather short time constants, on the order of days. The circulation model employs a monthly time step. We use an implicit scheme to solve the equations of the biological model. For small time steps its solution is identical to a more time consuming Runge-Kutta method. Increasing the time step to 1 month results in a strongly reduced variability in the biological variables. Therefore we use a time step of about 1 week (7.5 days) for the biological model and run it forward in time by four time steps, that is, 1 month. From the net changes in nutrients and plankton we determine the corresponding variations in other tracers (e.g., ΣCO_2, alkalinity, and silicate). The export flux out of the euphotic zone is integrated over the four weekly time steps and distributed over depth. All tracers are transported by the same advection and convection scheme using the monthly time step of the circulation model.

We start the new biological part with the minimum plankton concentration (P_{min}, Z_{min}) everywhere. The DOC concentration was set uniformly to 0.01 μmol C L^{-1} . All other values were taken from the simulations by *Maier-Reimer* [1993]. The efficient configuration of HAMOCC allows us to integrate the model to a final state very close to equilibrium (several thousand years) for any chosen parameter set. At this final state, fluxes between biological compartments (Figure 2) are almost perfectly balanced.

Table 1. Parameters of the Plankton Model in HAMOCC3.1

Parameter	Symbol	Unit	Value
	Phytoplankton		
Half-saturation constant for nutrient uptake	N_0	μmol P L^{-1}	0.016
Total incoming radiation	I_0	W m^{-2}	
Initial slope of P-I curve	α	m^2 (W d)$^{-1}$	0.025
Photosynthetically active radiation	PAR		0.40
Light extinction factor	k	m^{-1}	0.025
Minimum phytoplankton concentration	P_{min}	μmol C L^{-1}	0.01
Specific mortality rate	d_p	d^{-1}	0.008
Exudation rate of DOC	γ_P	d^{-1}	0.03
Maximum growth parameters	a	d^{-1}	0.6
	b		1.066
	c	$°C^{-1}$	1.0
	Zooplankton		
Half-saturation constant for phytoplankton ingestion	P_0	μmol C L^{-1}	4
Grazing rate	g_0	d^{-1}	0.9
Egestion as fecal pellets from herbivores	(1- ϵ_{her})		(1-0.8)
Assimilation efficiency	zinges		0.5
Excretion rate of DOC	γ_Z	d^{-1}	0.06
Specific mortality rate	d_z	d^{-1}	0.008
Egestion as fecal pellets from carnivores	(1-ϵ_{can})		(1-0.95)
Minimum zooplankton concentration	Z_{min}	μmol C L^{-1}	0.01
	Detritus		
Maximum remineralization rate of POC	l_0	yr^{-1}	0.24
	Dissolved Organic Carbon		
Maximum remineralization rate	d_0	d^{-1}	0.025
Half-efficiency constant of decay	k_d	μmol P L^{-1}	0.5
Redfield ratio of carbon to oxygen	$R_{C:O_2}$		122:-172
Redfield ratio of carbon to phosphate	$R_{C:P}$		122:1

3. Results

3.1. Biological Production

The biologically induced carbon fluxes within the euphotic layer (the upper 100 m) are shown in Figure 2. The annual global net primary production is 43.6 Gt C yr^{-1}. The amount of 11.1 Gt C yr^{-1} of this production is fueled by phosphate which is transported from deeper layers into the euphotic zone. This fraction of the production is defined as new production [*Eppley and Peterson*, 1979], in contrast to the regenerated production, which is based on nutrients recycled within the euphotic zone. In a steady state, new production has to be equal to the export of all organic material. In the current version of the model, about 8.8 Gt C yr^{-1} are exported out of the euphotic zone as POC, which consists mainly of fecal pellets and a smaller amount of phytodetritus. A remaining fraction of exported organic material leaves the surface layer by downward advection: about 1.7 Gt C yr^{-1} is transported to greater depth as dissolved organic carbon, 0.3 Gt C yr^{-1} is transported as phytoplankton and 0.3 Gt C yr^{-1} in transported as zooplankton. Below the productive zone, organic material is remineralized, and its inorganic components return to the euphotic zone by advection. A common measure for a biological regime is the f ratio, that is the ratio of new to total primary production as defined by *Eppley and Peterson* [1979]. Regions with high upwelling rates show generally a high f ratio, while in the oligotrophic regions of the subtropical gyres a low f ratio is found. Eppley and Peterson's global estimate of the f ratio is 0.1-0.2 which is based on a total primary production of 19.1-23.7 Gt C yr^{-1} and a new primary production of 3.4-4.7 Gt C yr^{-1}. The global average f ratio in our simulation is about 0.25 (new production:net primary production equals 11.1:43.6) which is

slightly higher than the number of Eppley and Peterson. With a given circulation field and a fixed distribution function for organic material the simulated new production has to stay within a certain range of possible values if we want to achieve a reasonable surface phosphate distribution. In steady state, export of organic material matches upward transport of nutrients. Allowing a higher export production depletes the surface layer of nutrients, whereas a low export production increases the surface nutrient level. Thus, with a given vertical distribution function for organic matter with depth, the values of export production and new production are constrained by model physics.

The pCO_2 variations mirror the seasonal turnover of organic matter within the surface layer. If a strong pCO_2 drawdown is observed, the equivalent amount of carbon must be stored in organic material, unless mixing or gas exchange accounts for the carbon loss. Consequently, the minimum annual net primary production can be derived from the pCO_2 seasonality. As stated above, the fate of the biogenically produced carbon is constrained by the circulation field. In view of simulating a realistic surface nutrient distribution only part of that biogenically produced carbon can be exported, or to put it the other way round, if we simulate only that fraction of biological production, that is exported (i.e., f ratio equals 1 which means total primary production equals new production), we can achieve no agreement between simulated and observed pCO_2-variations [*Maier-Reimer*, 1993]. In an earlier model version we achieve consistency with oceanic pCO_2 data only when simulating unrealistically high phytoplankton concentrations [*Kurz*, 1993]. That model version predicted a global f ratio of 0.5. A further independent test, that is, the analysis of the atmospheric seasonal oxygen cycle (see section 4) showed that the net primary production was rather underestimated in this previous model version. With a higher net primary production most of the regeneration of biogenic carbon has to take place within the euphotic zone. Higher export would result in a nutrient depletion of the surface. In our model, 15.7 Gt C yr^{-1} of the net primary production are respired by zooplankton activity, and 1.7 Gt C yr^{-1} are respired by carnivores, the next higher trophic level. The amount of 15.1 Gt C yr^{-1} is remineralized via the microbial loop, that is, the organically fixed carbon is excreted by zoo- and phytoplankton as DOC which, then, is oxidized by bacteria back to its inorganic components according to the assumed constant Redfield ratio.

3.2. Seasonal pCO_2 Variations

The most pronounced variations of the carbon quantities can be seen in the seasonal pCO_2 cycle. Unfortunately, the database of repeated seasonal pCO_2 measurements at a fixed location is up to now very sparse and all stations, available to us, are located in the northern hemisphere. Figure 3 displays measurements from different years around Iceland, the area of the North Atlantic Bloom Experiment (NABE), station P, and NW Pacific (symbols). Where available, the standard deviation is shown as well. The simulated seasonal cycle (solid line) lies within the range of observations at most stations. The strong pCO_2 drawdown around Iceland is well reproduced. The amplitude is slightly underestimated. At NABE the model predicts a spring pCO_2 reduction of about 50 ppm, slightly less than observed. The shape of the seasonal signal is well reproduced, but the model starts from a higher winter value than observed . Both the observed and simulated ΔpCO_2 signal at station P in the North Pacific (50°N 145°W) show only small seasonal variations (± 25 ppm). The model

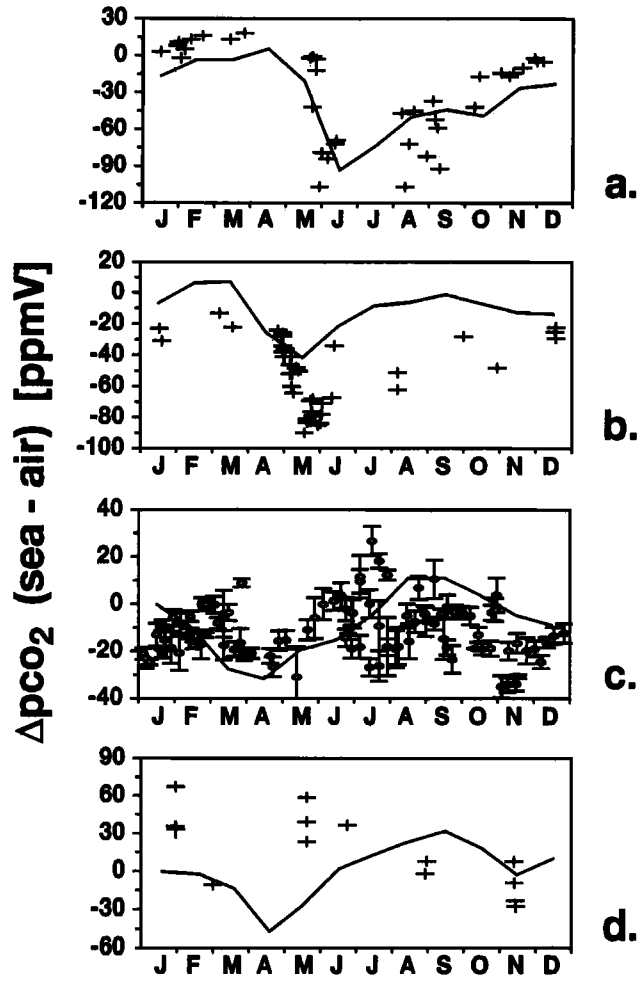

Figure 3. Seasonal cycle of ΔpCO_2 (in parts per million by volume) for stations in the North Atlantic: (a) Iceland (64°N 25°W) and (b) NABE (47°N 20°W) and the North Pacific: (c) station P (50°N 145°W) and (d) NW Pacific (40°N 160°E). Measurements are shown by symbols with standard deviation, if available. Solid line shows model results.

slightly overestimates the pCO_2 reduction in spring. However, the simulated values of the climatologically forced model lie well within the scatter of the data.

The fourth station is located in the North Pacific where high mixing rates in the winter months raise the ΔpCO_2, and biological production lowers ΔpCO_2 during summer. In the simulation, high winter values are missing. This insufficient reproduction is a result of a deficiency in the physical part of the model. In the present configuration the thermocline in that region is too shallow, as evidenced most clearly in a transient simulation of chlorofluorocarbons uptake by the ocean [*Maier-Reimer*, 1994].

To summarize, the model is generally able to simulate significant regional differences with one global parametrization. In the two stations in the northern Atlantic the rapid shallowing of the mixed layer triggers the phytoplankton blooming. The winter zooplankton concentration is very low at both stations. Thus grazing activity does not act as a growth limitation on phytoplankton at the beginning of the bloom. At station P, the seasonal change of the growth rate $r(T, L)$ is similar to that at NABE. However, at station P no strong vertical mixing occurs, and the predicted winter mixed layer is only around 90 m deep. Thus, during the winter months a higher standing stock of both phytoplankton and zooplankton is simulated. The improvement of the growth condition in spring leads to an increase in phytoplankton productivity, but the abundance of zooplankton inhibits changes in the standing stock of phytoplankton. The increased phytoplankton productivity results immediately in a higher zooplankton concentration. Grazing control in the open subarctic ocean is discussed currently as an explanation for "high-nutrient low-chlorophyll" areas (HNLC areas) [*Frost*, 1987]. The model setup supports this controlling mechanism. However, another explanation for the existence of HNLC areas is a growth limitation of phytoplankton because of lack of iron [*Martin et al.*, 1990]. To date the complete cycling of iron is not well understood within the scientific community. Therefore it is beyond the scope of this study to investigate which of the two processes control the HNLC areas.

3.3. Surface Tracer Distribution

3.3.1. Phosphate. The comparison of observed and simulated global nutrient distributions gives insight into the effects of the biological production scheme. Figure 4a shows the annual mean surface phosphate distribution as predicted by the model. The simulated large-scale structures are in good agreement with thoses compiled from observations (not shown here, see *Najjar et al.* [1992]). The most prominent feature is the high phosphate concentration in Equatorial Pacific upwelling area which is broader in north-south direction and extends farther to the west in the model (0.5 μmol P L^{-1} at about 150°E instead of 160°W [see *Conkright et al.*, 1994]. This deficiency might be connected with the physical part of the model. Equatorial upwelling is a result of the imposed wind stress. We use the common wind stress data set from *Hellermann and Rosenstein* [1983]. These data give higher wind stress values for the equatorial region than ECMWF model analyses derived from observations.

For a more rigorous comparison we again extracted simulated values at the same time and location as available measurements (Figures 4b and 4c). Both transects show a remarkable agreement between simulated and observed values for all regions besides the North Pacific. Since we do not use any restoring toward observations, the nutrient distribution is the result of the ocean dynamics and the assumed biological production scheme. A too strong biological export production, for instance, would result in an unrealistic nutrient depletion in the subtropical gyres. On the other hand, weaknesses of the transport model are still visible in the nutrients distribution. As stated earlier, the physical model overestimates the stratification in the North Pacific. This results in surface nutrient concentration and ΔpCO_2 (Figure 3d) during the winter months that are lower than observed.

3.3.2. Chlorophyll. The model simulates organic material in four components: phytoplankton, zooplankton, dissolved organic carbon (DOC), and detritus (POC), of which the last only exists below the euphotic zone. A direct comparison with mapped data is feasible only for phytoplankton concentrations which can be converted to chlorophyll concentrations. These can then be compared to data derived from satellite imagery of the coastal zone color scanner (CZCS) [*Feldman et al.*, 1989]. As the conversion factor we assume a time and space independent chlorophyll-to-carbon mass ratio of 1 to 60. Figures 5a and 5b show the average observed and simulated values for two seasons (April to June and October to December). The overall pattern of chlorophyll distribution is qualitatively reproduced. Higher chlorophyll concentrations are simulated during the productive season in each hemisphere. Equatorial concentrations are low all year round. The simulated equatorial concentrations are twice as high as the observations. However, one has to keep in mind that the simulation give average values of the top 50 m, while the satellite measures concentrations in the upper 10-20 m of the water column. The satellite detection level of the CZCS is of the order of a decimeter depending on the turbidity by particles [*Gordon et al.*, 1982]. Here, in stratified and well-illuminated waters the highest concentration of phytoplankton is found at greater depth (> 25 m)[*Lindley et al.*, 1995]. This subsurface chlorophyll signal cannot be captured by the sensors.

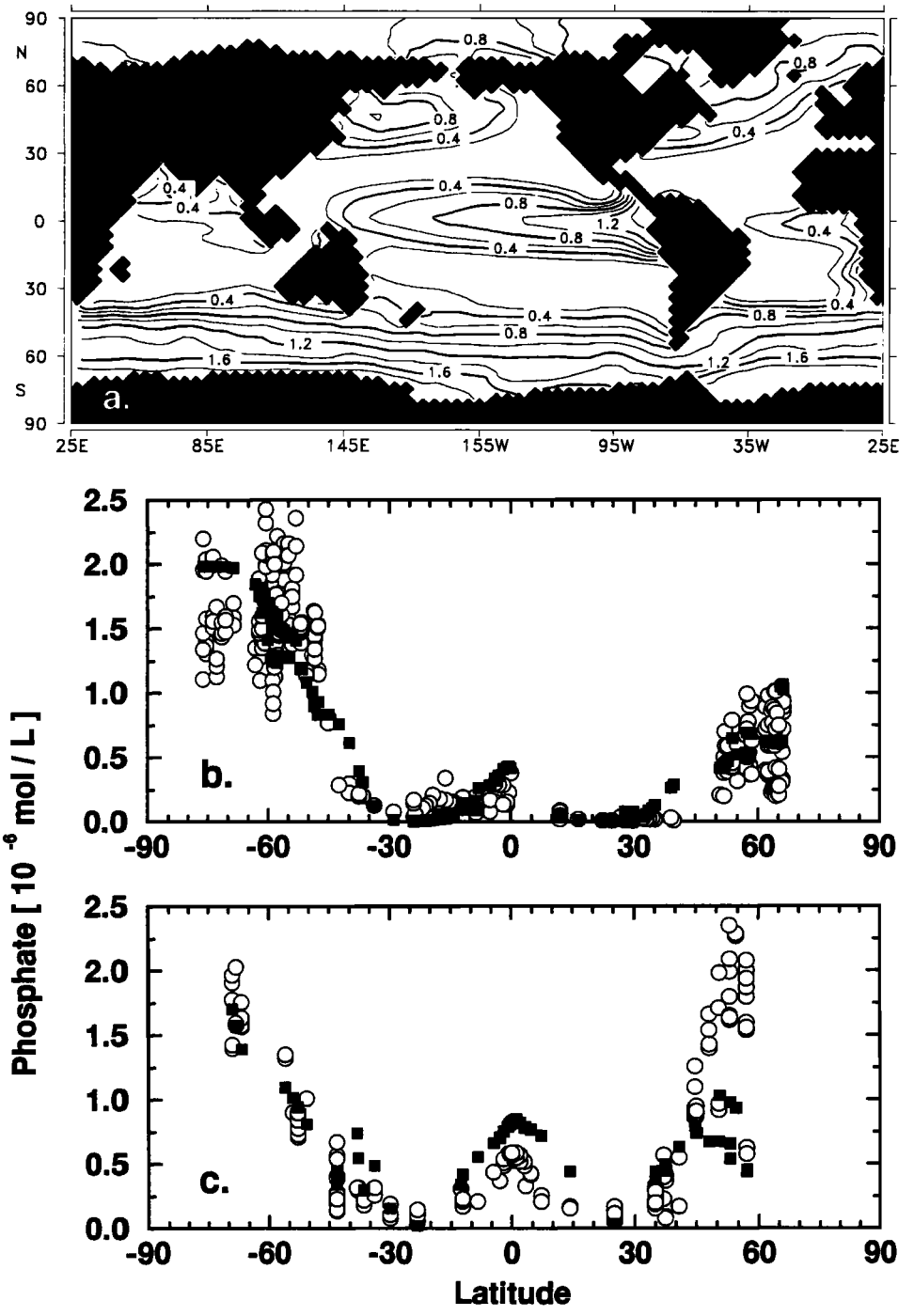

Figure 4. (a) Simulated annual mean surface phosphate concentration (in μmol P L^{-1}). Isoline spacing is 0.2 μmol P L^{-1}. Simulated values (squares) and observations (open circles) [*Conkright et al.*, 1994] along a north-south transect in (b) the Atlantic (30°W) and (c) the Pacific (180°) are shown. Simulated values are extracted at the same times and locations as measurements.

The extreme low chlorophyll concentrations (Chl) of less than 0.05 mg Chl m^{-3} observed in the subtropical gyres are not simulated by the model. However, the model produces a very similar meridional gradient between 30°N and 30°S (Figure 6). The annual mean chlorophyll concentration in the Equatorial Pacific between 150°E and 90°W decreases by 0.05 mg Chl m^{-3} toward the subtropical gyres in the observations as well as in the model.

The high chlorophyll concentrations on shelf areas can not be reproduced by the model since these areas are not resolved (Figures 5a and 5b). The apparent

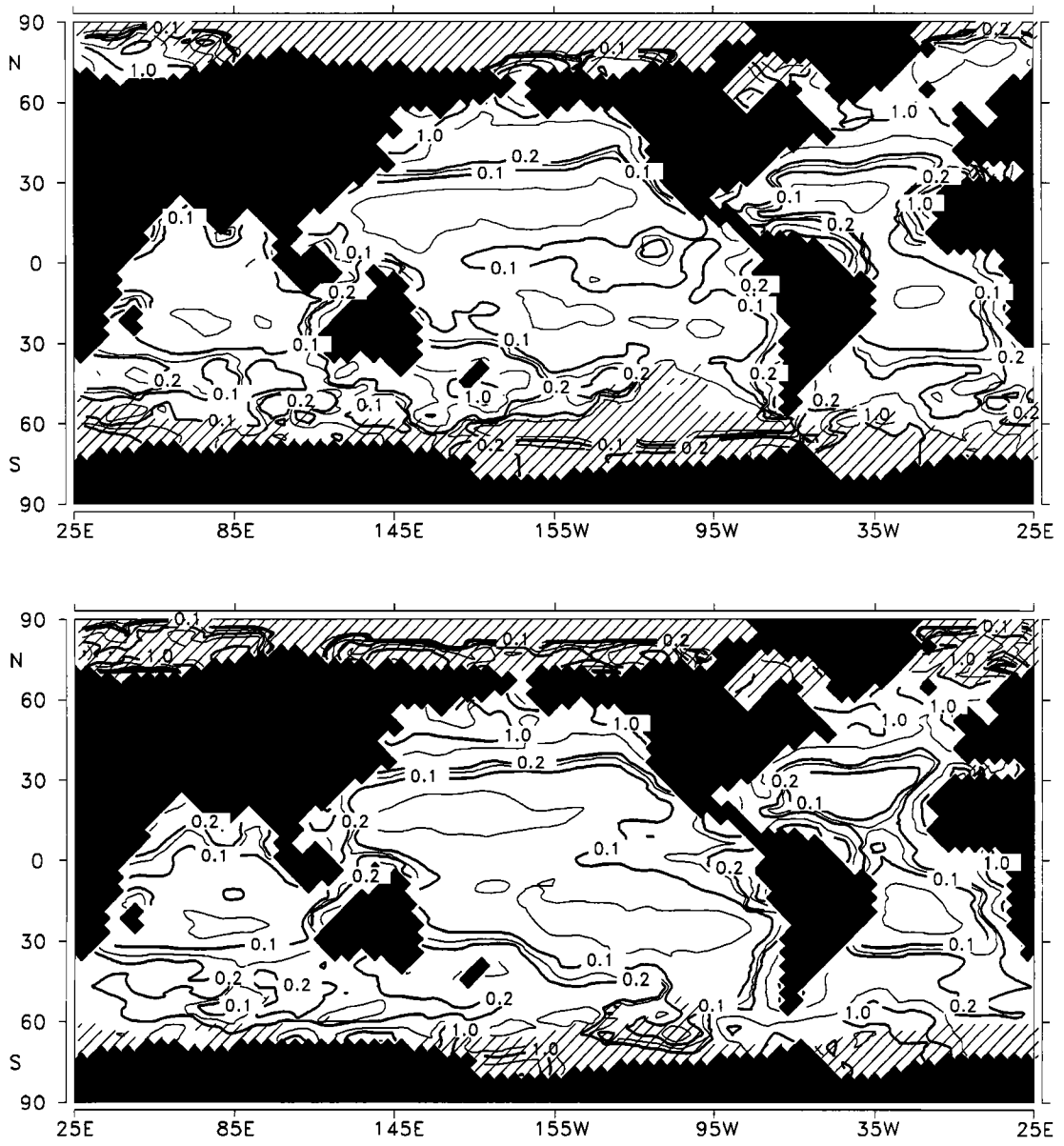

Figure 5a. Seasonal mean of the chlorophyll distribution (in mg Chl m^{-3}). Observations from the coastal zone color scanner (CZCS) [*Feldman et al.*, 1989] are interpolated onto model grid. Isolines are at 0.05, 0.1, 0.15, 0.2, 0.5, 1, 2, and 5. Two seasons are shown: April - June (top) and October - December (bottom). Hatched areas are regions where no or only one data point per grid cell was available for the interpolation.

high chlorophyll values in the vicinity of river outlets are mainly identified as terrigenous substances (e.g., Gelbstoff) and are therefore not part of the simulation.

North of 45°N the concentrations increase in the April-to-June interval because of spring bloom conditions. Concentrations of > 1.0 mg Chl m^{-3} are located in the North Atlantic in the same region as in the data. The observed maximum concentration of > 2.0 mg Chl m^{-3} north of Iceland is not reproduced by the model. In October to December the satellite measurements show values higher than 0.5 mg Chl m^{-3} north of 40°N in the Atlantic which are not present in the model. However, with low incident irradiance, satellite data become more questionable. In situ measurements made at various stations during these months show rather low chlorophyll concentrations [*Yoder et al.*, 1993], as predicted by the model. At ocean station I (59°N, 19°W), in situ measurements show a decrease from 0.8 mg Chl m^{-3} in October to 0.1 mg Chl m^{-3} in December. The model gives winter values around 0.1 mg Chl m^{-3} but does not simulate the October high. The CZCS data at that station are only available for October and give a

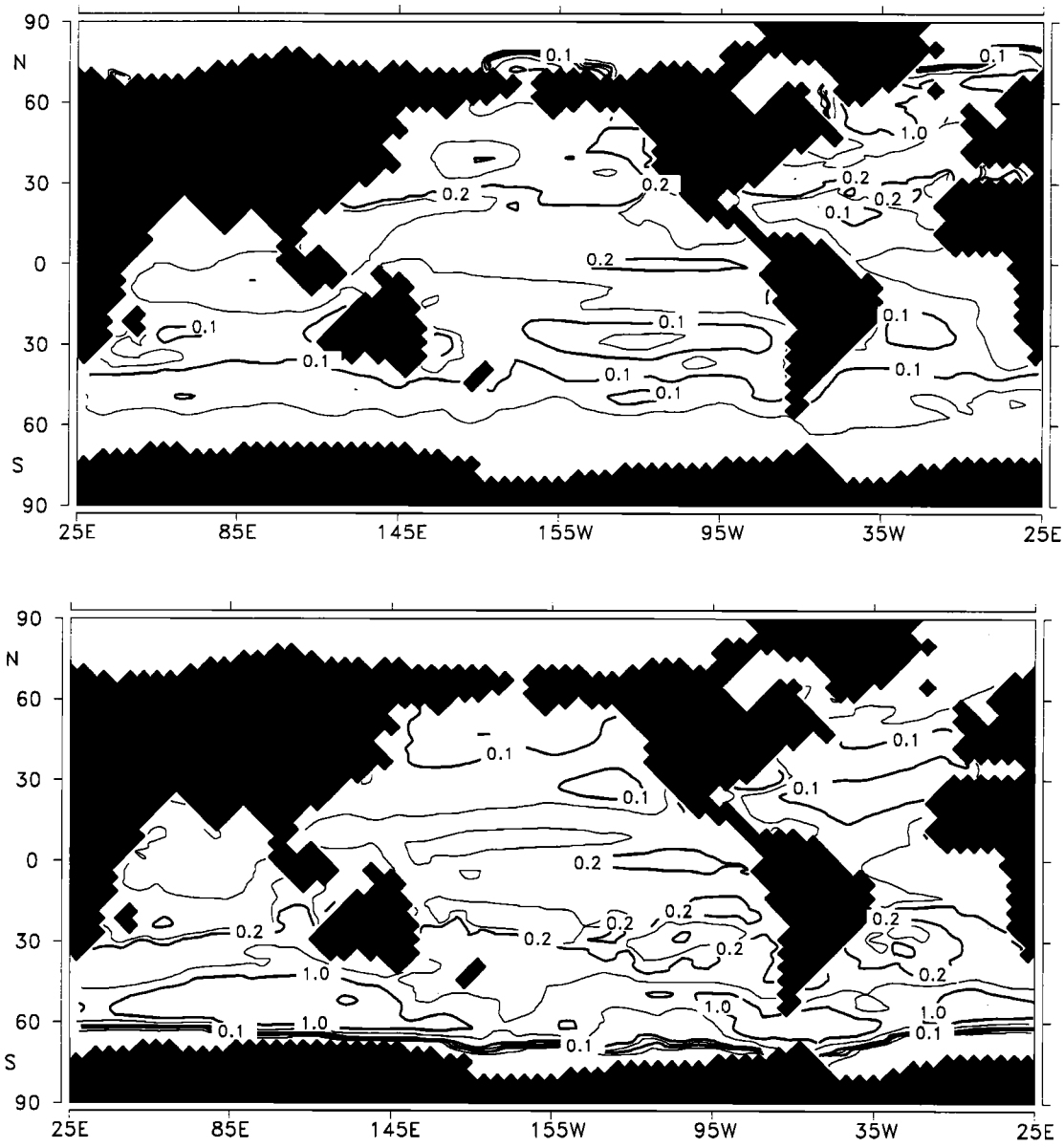

Figure 5b. Result of HAMOCC3.1. Chlorophyll values were derived from phytoplankton concentration by assuming a C:Chl mass ratio of 60:1. Same seasons and isolines as in Figure 5a are displayed.

chlorophyll concentration of 1.8 mg Chl m^{-3}. A similar feature is observable at ocean station P (50°N, 145°W). Values derived from the CZCS are 0.6 mg Chl m^{-3} in September and increase to 3.0 mg Chl m^{-3} until December, while in situ measurements give values of less than 0.3 mg Chl m^{-3} all year round. Simulated values range from 0.1 to 0.3 mg Chl m^{-3} during the whole year with the exception of a higher concentration (0.7 mg Chl m^{-3}) in March.

One dominant feature in the simulation is the high chlorophyll concentration in October to December in the southern hemisphere south of 40°S with values higher than 1.0 mg Chl m^{-3}. This is not present in the CZCS data. The comparison of in situ data south of 30°S with the corresponding CZCS data [*Sullivan et al.*, 1993] show, that the CZCS data are underestimated by about a factor of 2. Zonally averaged chlorophyll measurements from 30°S to 60°S ranged between 0.2 and 1.2 mg Chl m^{-3} in October to March. The model predicts similar values for the same time and location.

An additional uncertainty in this comparison originates from the assumed fixed ratio of chlorophyll to carbon. *Antia et al.* [1963] measured the C:Chl ratio during an algae bloom and found a doubling of the ratio

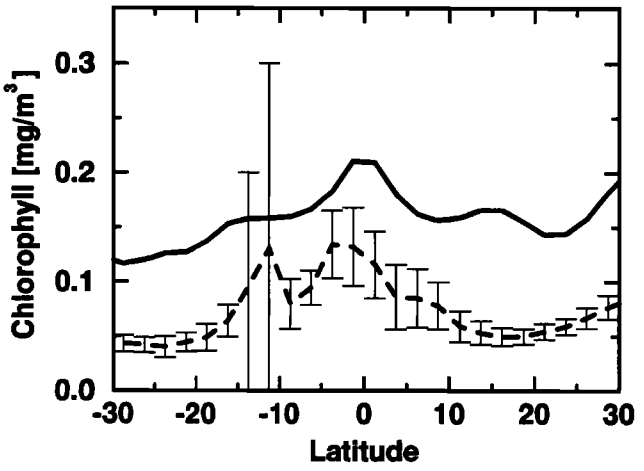

Figure 6. Annual mean chlorophyll distribution along 140°W between 30°S and 30°N (in mg Chl m^{-3}). Dashed line indicates satellite observations interpolated onto model grid and their average monthly standard deviation (CZCS [*Feldman et al.*, 1989]); solid line indicates model results

at the end of the bloom. In view of the uncertainties of the CZCS data and the simplicity of the plankton model the aggrement between observation and simulation is reasonably good.

To illustrate the seasonal variations of the different biological compartments, we show concentrations of phytoplankton, zooplankton, and dissolved organic carbon and export production as zonal averages for the Pacific in a time versus latitude diagram (Plate 1). Two years are shown. In all properties only small seasonal variations are simulated at the equator. Steady supply of nutrients and nearly uniform growth conditions result in a constant standing stock of phytoplankton and zooplankton. Small undulations, mainly present in the zooplankton concentration, reflect variations of the upwelling velocity because of the prescribed wind stress forcing and thus a variable transport of nutrients into the euphotic zone.

In the low latitude regions the growth conditions vary slightly with season ($r(T, L)$ = 0.8 - 1.2 d^{-1}) (Plate 2), but because of low nutrient concentration in the subtropical gyres (< 0.2 μmol P L^{-1}) only a small plankton stock can be supported. Plankton concentrations in higher latitudes show distinct seasonal variations. There is a time lag of about a month between the maxima of the phytoplankton and the zooplankton concentration. At 35°N the peak of the phytoplankton bloom is in April with a corresponding maximum of zooplankton in May. In both plankton concentrations the seasonal poleward propagation of the spring bloom can be identified. The maximum export production occurs simultaneously with the maximum zooplankton concentration indicating that the major fraction of exported organic material consists of fecal pellets. Since DOC is assumed to be mainly excreted by zooplankton, DOC concentration starts to increase with increasing zooplankton.

There is a simulated north-south asymmetry of the maximum height of seasonal peaks in all tracers. Phytoplankton growth conditions are a function of temperature, incident light, and mixed layer depth. The latter shows the strongest difference between the northern and southern hemisphere (Plate 2) with mixed layer depths of more than 150 m in the southern hemisphere during most of the year. For example, at 60°S and 165°E the average growth factor in the surface is higher than 0.5 d^{-1} only in January, while in the corresponding northern latitudinal band, values higher than 0.6 d^{-1} are present from May to August.

3.3.3. DOC. In our simulation we included a short-living organic component (dissolved organic carbon (DOC)). It is excreted by plankton and passively transported by the water movement because of its small size (methodically all organic carbon that passes a 0.2 - 1-μm filter is defined as DOC). DOC is oxidized by microbial activity. However, there is a large fraction of DOC within the ocean that has a high ^{14}C age. This refractory part of DOC with a typical concentration of about 40 μmol C L^{-1} [*Murray et al.*, 1994; *Copin-Montégut and Avril*, 1993] is nearly homogeneously distributed with depth and is not considered in our simulation. For the seasonal cycle the more labile fraction is relevant which has a typical decay rate of days to weeks [*Amon and Benner*, 1994; *Kirchman et al.*, 1991]. In the course of a year it has been observed that wintertime DOC concentrations increased during spring and summer and nearly doubled in autumn [*Copin-Montégut and Avril*, 1993]. About 40 μmol C L^{-1} have been incorporated into the seasonal DOC pool in the eastern North Atlantic (47°N, 20°W) [*Bodungen and Kähler*, 1994]. This is a considerable change in a nonliving carbon pool; for comparison, measurements of the dissolved inorganic carbon concentration at NABE (47°N, 20°W) display a reduction of about 30 μmol C L^{-1} during a spring bloom [*Chipman et al.*, 1993]. In our simulation the DOC concentration increases at NABE from 5 μmol C L^{-1} in February to 33 μmol C L^{-1} in August. The concentration change is related to the increase in the zooplankton concentration, which is the major DOC producer according to the parametrization.

The nutrient dependency of bacterial uptake of DOC, that is, the decay of DOC, has been described by *Kirchman et al.* [1991]. The formulation we used here has no significant influence on the seasonal cycle of pCO_2. Variations of the half-saturation constant k_d (e.g., reducing it by a factor of 10) result only in a change of the DOC pool size and the global DOC distribution. In the Equatorial Pacific the DOC concentration increases by 15 μmol C L^{-1} from the equator toward 15°N and 15°S (Plate 1). A similar gradient has been observed

by *Murray et al.* [1994] in that region. With a weaker dependency on the nutrient concentration (smaller k_d) the DOC gradients are reduced.

We like to emphasize that this seasonally varying DOC pool is not comparable with that used in previous 3-D studies on the carbon cycle [*Najjar et al.*, 1992; *Bacastow and Maier-Reimer*, 1991]. It has a much shorter turnover rate and, correspondingly, a smaller pool size of about 8 Gt C. In experiments with long-living DOC, average surface values of more than 150 μmol C L^{-1} were predicted. This was in accordance with the measurements of *Sugimura and Suzuki* [1988], which have been withdrawn [*Suzuki*, 1993]. Recent observations give only DOC values of 60 to 80 μmol C L^{-1} during peak times [*Murray et al.*, 1994; *Bodungen and Kähler*, 1994]. A long lifetime of DOC has the appreciable effect of reducing the horizontal gradients in the Equatorial Pacific region, but it also obliterates the large-scale structure of the nutrient and $\delta^{13}C$ fields.

3.4. Tracer Distribution Along Vertical Cross Sections

One of the most apparent deficiencies in previous 3-D ocean models of the biological pump is the effect of nutrient trapping below the thermocline in the Equatorial Pacific [*Najjar et al.*, 1992; *Maier-Reimer*, 1993] In their models the interaction of the upwelling regime and prescribed biological production scheme results in an unrealistic accumulation of nutrients in the East Equatorial Pacific. The upward transport brings nutrients in the euphotic zone where they are incorporated into organic material because of optimal growth conditions. In these particle-only models this organic matter sinks to greater depth according to prescribed distribution function [*Suess*, 1980; *Martin et al.*, 1987]. Its remineralization consumes oxygen and releases nutrients. Phosphate concentration of more than 4.5 μmol P L^{-1} are simulated off the coast of Central America [*Maier-Reimer*, 1993; *Najjar et al.*, 1992]. Accordingly, the oxygen distribution at depth shows an extreme oxygen deficiency.

In the real ocean the apparent lack of oxygen to degrade all organic material is partly compensated by the process of nitrate or sulfate reduction which is not considered in our model. *Codispoti and Christensen* [1985] estimated that one third of the total nitrogen loss in the world ocean occurs by denitrification in the East Equatorial Pacific. *Toggweiler and Carson* [1995] stated that the nitrogen sink by particle export might be comparable to the loss of nitrate by denitrifying bacteria in this region. *Devol* [1991] estimated from observations that annually about 60-80 Tg N are involved in denitrification processes.

If instantaneous remineralization and denitrification is prescribed in the anoxic regions of our model, we would need a rather unrealistically high amount of nitrogen (280 Tg N yr^{-1}) if we assume complete reduction of NO_3^- to N_2. On the basis of the used remineralization scheme with a POC decay time constant of approximately 4 years, we require only 32 Tg N yr^{-1} to ensure the decay of all POC within the zone where remineralization is stopped because of a lack of oxygen. This nitrogen demand is substantially lower than Devol's estimate, indicating that the decay POC is too slow. Increasing the decay rate affects the nitrogen demand, but the distribution of total phosphate, that is, the sum of organic and dissovled phosphate, is unchanged. As long as denitrification processes are generally not well enough understood, we see no advantage of including them into our model.

The nutrient trapping in particle-only models is mainly a result of an oversimplified biological production scheme, where the available nutrients are rapidly incorporated into organic material and entirely exported to depth. Figure 7 shows the predicted export production of HAMOCC3 and HAMOCC3.1 with the strongest changes in the equatorial region. In HAMOCC3 the zonal average export production is 70 g C m^{-2} yr^{-1} at the equator and drops down to about 10 g C m^{-2} yr^{-1} in the subtropical gyres. In HAMOCC3.1 the export production at the equator is reduced to some 40 g C m^{-2} yr^{-1}. The value in the subtropical gyres is similar to HAMOCC3. Thus, in HAMOCC3 there is a factor of 5 to 6 between high and low export production regimes, while in HAMOCC3.1 there is only a factor of 3. This lower ratio is also supported by the export production estimates of *Berger et al.* [1987] and *Eppley and Peterson* [1979].

Comparison with direct measurements of particulate carbon flux are difficult. *Murray et al.* [1994] observed in the Equatorial Pacific at 140°W a carbon flux of 3.2 mmol C m^{-2} d^{-1} in February and 11.8 mmol C m^{-2} d^{-1} in August with drifting traps. Our predicted particulate carbon flux is 12.5 mmol C m^{-2} d^{-1} in February, which is 4 times higher than observed. In August the model simulates a POC flux at 140°W of 13.5 mmol C m^{-2} d^{-1}. This corresponds well with the observed values from drifting traps. The higher carbon fluxes occurred in the Pacific when an elevated concentration of diatoms were observed. The biological conditions observed in August seemed to be closer to the model's design and therefore correspond better. The lack of diatoms in February might be related to a lack of iron, but temporal variations in species and size composition are not included in the model. We note, however, that estimates of the POC flux with the ^{234}Th method in that region give substantially lower values for both months. Thus estimates of the POC flux are rather uncertain. If we were to quantify the overall misfit between model and data, we would attribute a much smaller weight to

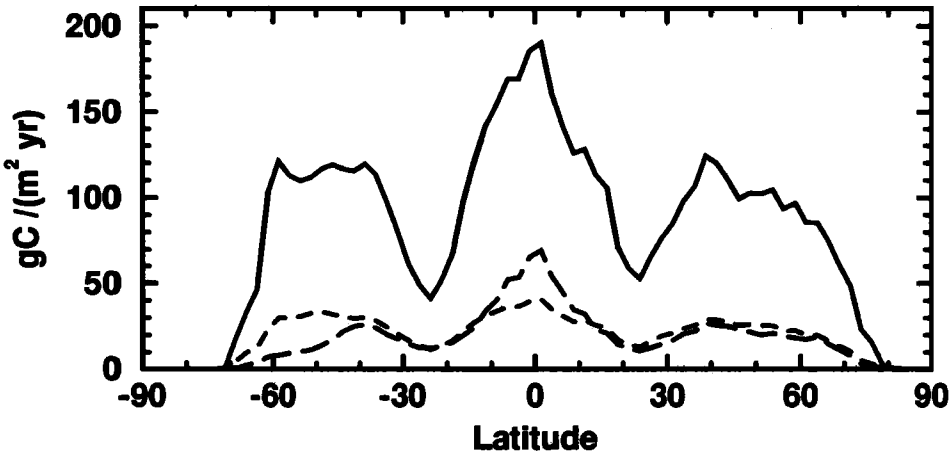

Figure 7. Annual global zonal average of net production (solid line) and of export production (dashed line) from HAMOCC3.1 (μmol C m^{-2} yr^{-1}) versus latitude. For comparison the annual global zonal average of export production from HAMOCC3 (long-dashed line) is also shown.

the discrepancy in these fluxes than, for instance, to a discrepancy in the phosphate distribution.

The reduced equatorial export production in HAMOCC3.1 compared to HAMOCC3 is a result of the zooplankton activity. In HAMOCC3, export production relied only on the local growth conditions and the supply of nutrients, which both show a maximum in the equatorial region. In this model version, zooplankton activity places an additional limit on phytoplankton growth. Nearly steady state conditions support a high standing stock of zooplankton which again keeps phytoplankton concentration low. Additionally, zooplankton is the main producer of DOC. This results in elevated DOC concentrations. To a large extent the lateral export of organic matter from equatorial regions is in the form of DOC (Figure 8). Phosphate is advected from north and south into the equatorial upwelling region. This convergence is compensated by a return flux of organic matter, mainly as DOC. A much smaller fraction is advected as particulate organic matter (POC). There is nearly no meridional transport of phytoplankton in any ocean basin (always less than 0.2 kmol P s^{-1}). Meridional transport of zooplankton is only important close to the equator, where the highest standing stock is also predicted. Advection of debris in noticeable quantities ($\approx$ 1 kmol P s^{-1}) is also related to the equatorial divergence and is a consequence of the assumed remineralization function with a time constant of 4 years. We choose the same function as in earlier version of HAMOCC3 in order to make a better comparison [*Maier-Reimer*, 1993]. However, particle transport within the ocean will be revised in the scope of a new

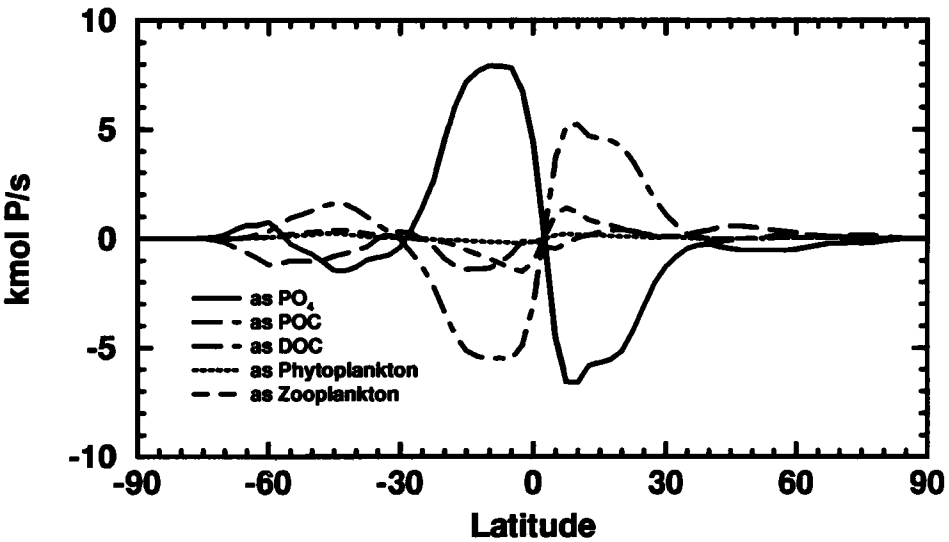

Figure 8. Global northward transport of phosphate as dissolved inorganic phosphate and fixed in various organic components. All are shown in kmol P s^{-1}.

sediment component which is developed for HAMOCC3 (E. Maier-Reimer, manuscript in preparation, 1996)

The roughly halved flux of organic material to greater depth at the equator has implications for the underlying nutrient and oxygen concentrations, as mentioned before. Figure 9 shows the total phosphate concentration (i.e., the sum of inorganic and organic phosphate) at 800 m depth. Off the coast of Central America there are total phosphate concentrations of more than 5 μmol P L^{-1} predicted in HAMOCC3 [see *Maier-Reimer*, 1993, Figure 14b; *Najjar et al.*, 1992]. In HAMOCC3.1 the highest total phosphate concentrations are also found in this region, but the values are less than 3.8 μmol P L^{-1} at 800 m. Correspondingly, the area with an oxygen deficiency decreases (not shown). In the Bay of Bengal, where no denitrification is observed in nature, the unrealistic oxygen deficiency, as predicted by HAMOCC3, disappears.

Figures 10a and 10b show annual mean Pacific zonal averages of total phosphate and oxygen saturation. Generally, observations and model simulations are in good agreement. The local extremes (a minimum in oxygen saturation and maximum in total phosphate) are confined to the equator, while in the observations they are located at the northern boundary. Simulated surface PO_4 values in the North Pacific are lower than in the observations north of 40°N. As stated above, this is related to the too stable stratification of the water column. It also shows up in a shallower O_2 ventilation than observed. At 40°S the Antarctic intermediate water brings oxygen to greater depths which is indicated by the elevated oxygen saturations at 750 m depth. In the LSG no Antarctic intermediate water is predicted for the Pacific. The higher ventilation of the waters at 30°S might affect the predicted oxygen minimum at the equator.

3.5. Air-Sea Flux

The impact of the plankton dynamic on the local air-sea fluxes of CO_2 can be estimated in the model, but there is hardly any evaluation with observations possible. The measurement of the natural fluxes is difficult since they are small because of the CO_2 buffering characteristics of sea water and the slowness of its gas exchange. Any variations in the atmosphere due to air-sea fluxes are spread out by the high zonal mixing rate of the atmosphere.

However, the linkage of carbon uptake and oxygen release during biological production provides a powerful constraint to test the model: since gas exchange processes are fast for gases with low solubility, the oxygen from biological production leaves the surface waters and imprints the signal on the atmosphere. Recent measurements of seasonal oxygen to nitrogen variations show amplitudes up to 100 per meg (1 per meg = 10^{-6}; 100 per meg are roughly a 20 ppm change in O_2) in the atmosphere [*Bender et al.*, 1996; *Keeling and Shertz*, 1992]. The signal is a combination of contributions from O_2 exchange between terrestrial biosphere and atmosphere and between ocean and atmosphere. The oceanic flux arises from biological production and from temperature dependent solubility changes. The solubility changes for nitrogen also effect the O_2/N_2 ratio and have therefore to be taken into account. On the basis of HAMOCC3.1 we calculated oxygen and nitrogen fluxes across the air-sea interface and used them as lower boundary conditions for an atmospheric transport model [*Heimann and Keeling*, 1989; M. Heimann, personal communication, 1993]. The terrestrial biosphere fluxes were taken from *Knorr and Heimann* [1995]. We limited our comparison to Cape Grim where the record contains nearly no signal from terrestrial sources or

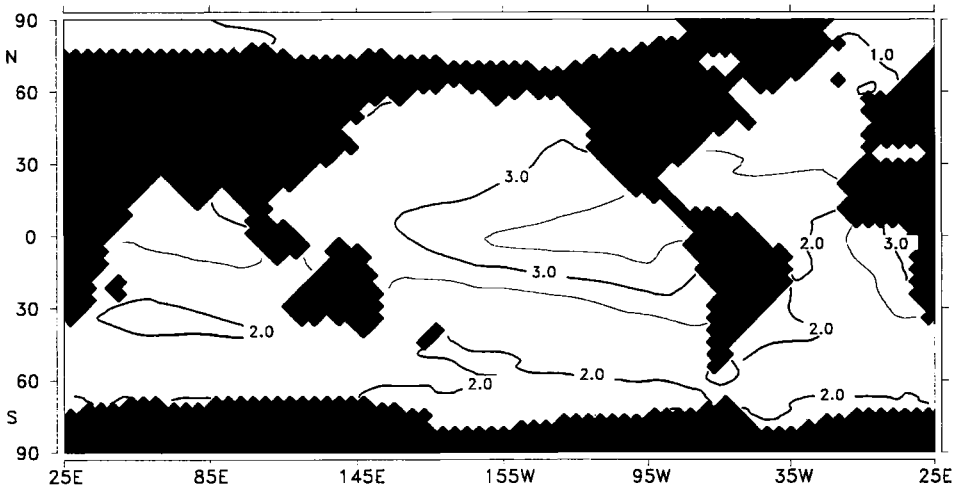

Figure 9. Total phosphate concentration at 800-m depths (in μmol P L^{-1}) in HAMOCC3.1. Total phosphate is the sum of organically fixed and dissolved inorganic phosphate.

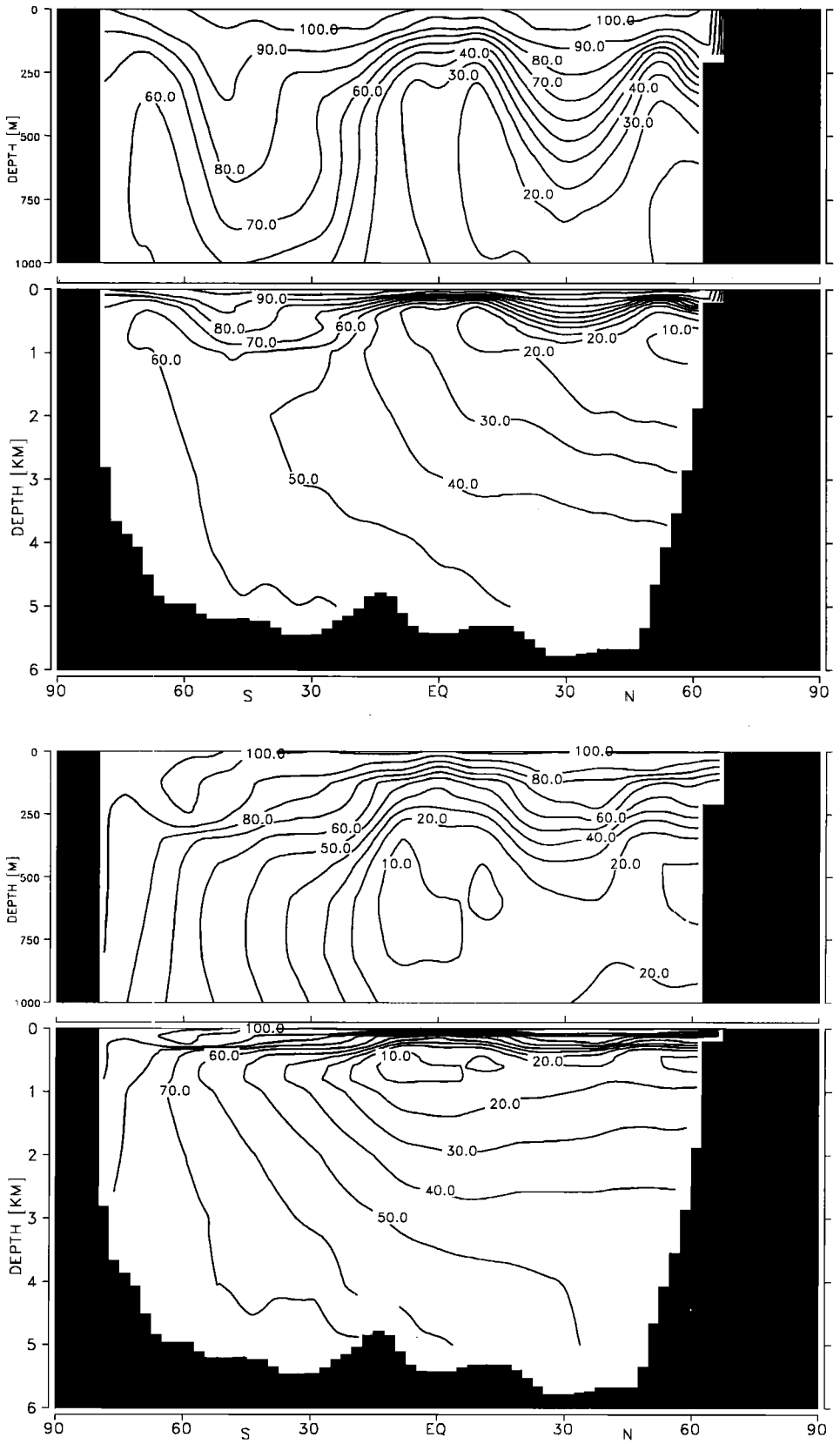

Figure 10a. Annual Pacific zonal average of oxygen saturation (in percent): (top) observations [*Levitus and Boyer*, 1994] interpolated onto model grid and (bottom) HAMOCC3.1. The upper kilometer is shown again with enlarged scale.

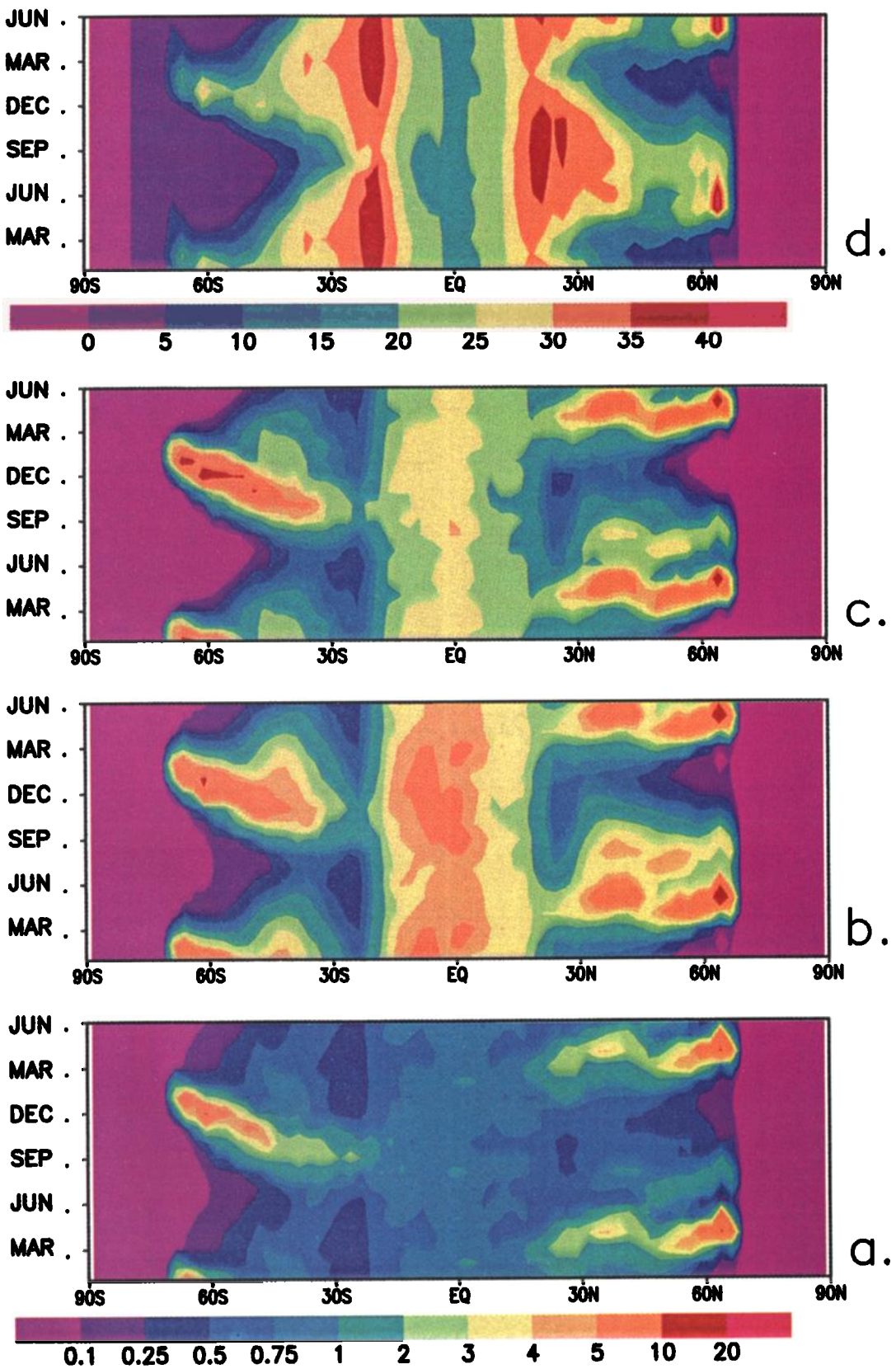

Plate 1. Time versus latitude of zonally averaged organic carbon pools in the Pacific: (a) phytoplankton, (b) zooplankton, (c) export production, and (d) dissolved organic carbon. All are shown in μmol C L^{-1}, except export production which is shown in μmol C L^{-1} $month^{-1}$

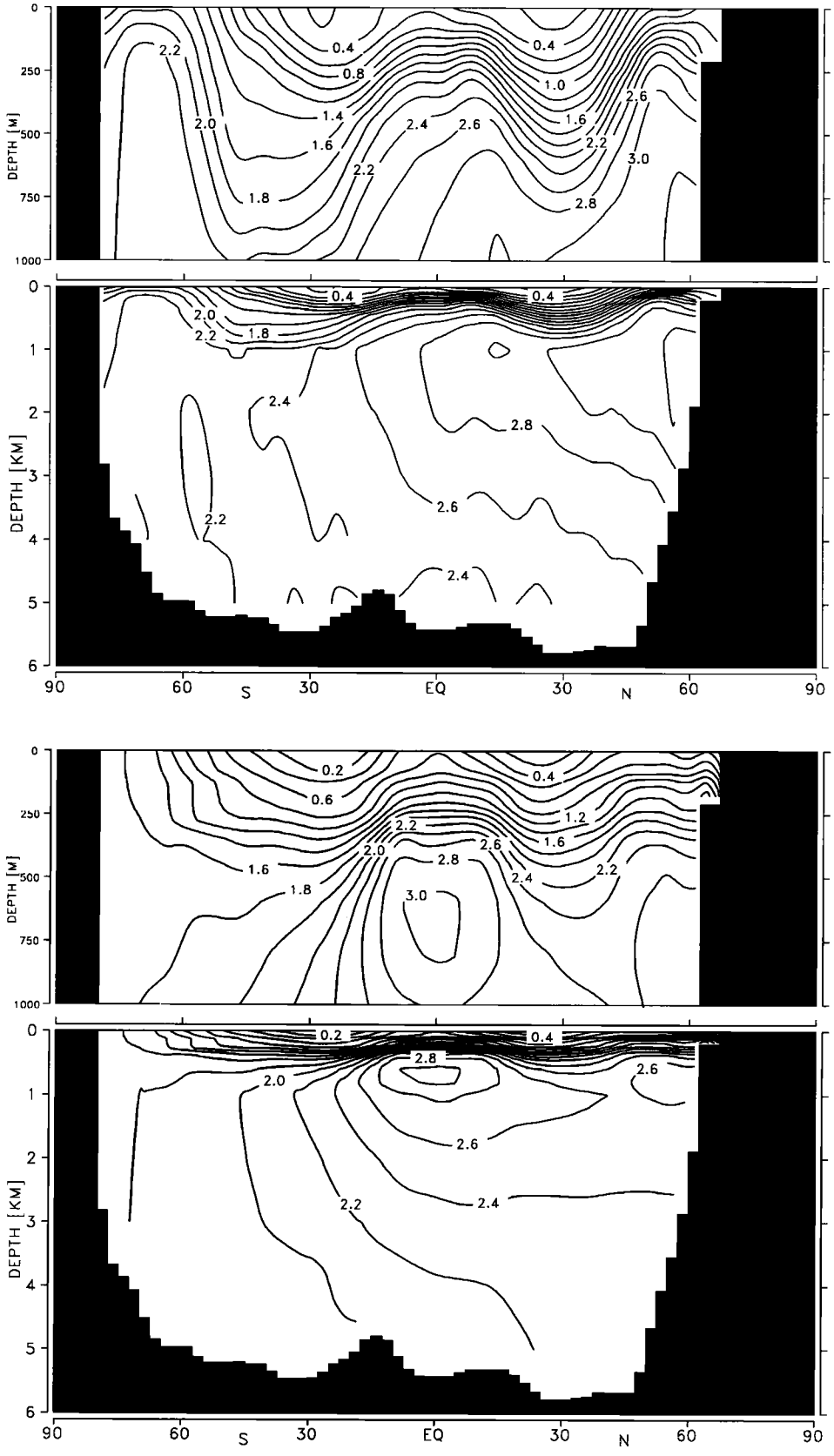

Figure 10b. Annual Pacific zonal average of phosphate (μmol P L^{-1}): (top) observations [*Conkright et al.*, 1994] interpolated onto model grid and (bottom) HAMOCC3.1. The upper kilometer is shown again with enlarged scale.

sinks (Figure 11). The shape of the curve is in very good agreement with the observations. The rapid O_2/N_2 increase in southern hemisphere spring because of outgassing of oxygen produced by the marine biota is followed by a slow decrease, when decay of biogenic matter and ocean mixing reduce the oxygen content in the surface layer. The amplitude is well reproduced, but the signal precedes the data by about 1 to 2 months. The accordance of the amplitudes indicates that the seasonal turnover of organic matter is well simulated by the model, but the timing of the biological activity seems to be displaced. The relatively long time step of the model can cause this displacement. An additional phase shift might result from our sampling technique. We calculated monthly averages from all predicted values, while measurements at Cape Grim are only sampled under certain wind conditions. *Ramonet* [1994] showed in a different study based on the same atmospheric model that a 2-month shift of the maximum pCO_2 concentration occurs when applying this selective sampling technique at Cape Grim.

Despite these phasing uncertainties we emphasize that atmospheric oxygen data provide an independent test for marine biota models. It is a unique quantity that gives an information about net carbon production in the plankton community. These measurements might help to constrain the biological component of carbon cycle models, especially in the remote areas of the Southern Ocean where in situ measurements of the seasonal variations of biological variables are very sparse. We will investigate additional locations to get more insight into the oceanic contribution to the observed oxygen signal (M. Heimann et al., manuscript in preparation, 1996).

4. Summary and Conclusion

The seasonal variation of surface pCO_2 is a result of strong biological activity in many regions. To get a dynamically consistent field of the oceanic pCO_2, we developed a very simple plankton model and embedded it into the Hamburg model of the oceanic carbon cycle (HAMOCC3). We consider our carbon cycle model as an element of a full climate model which should also be applicable to other climate states. Therefore we avoid any regional tuning and base the plankton model on

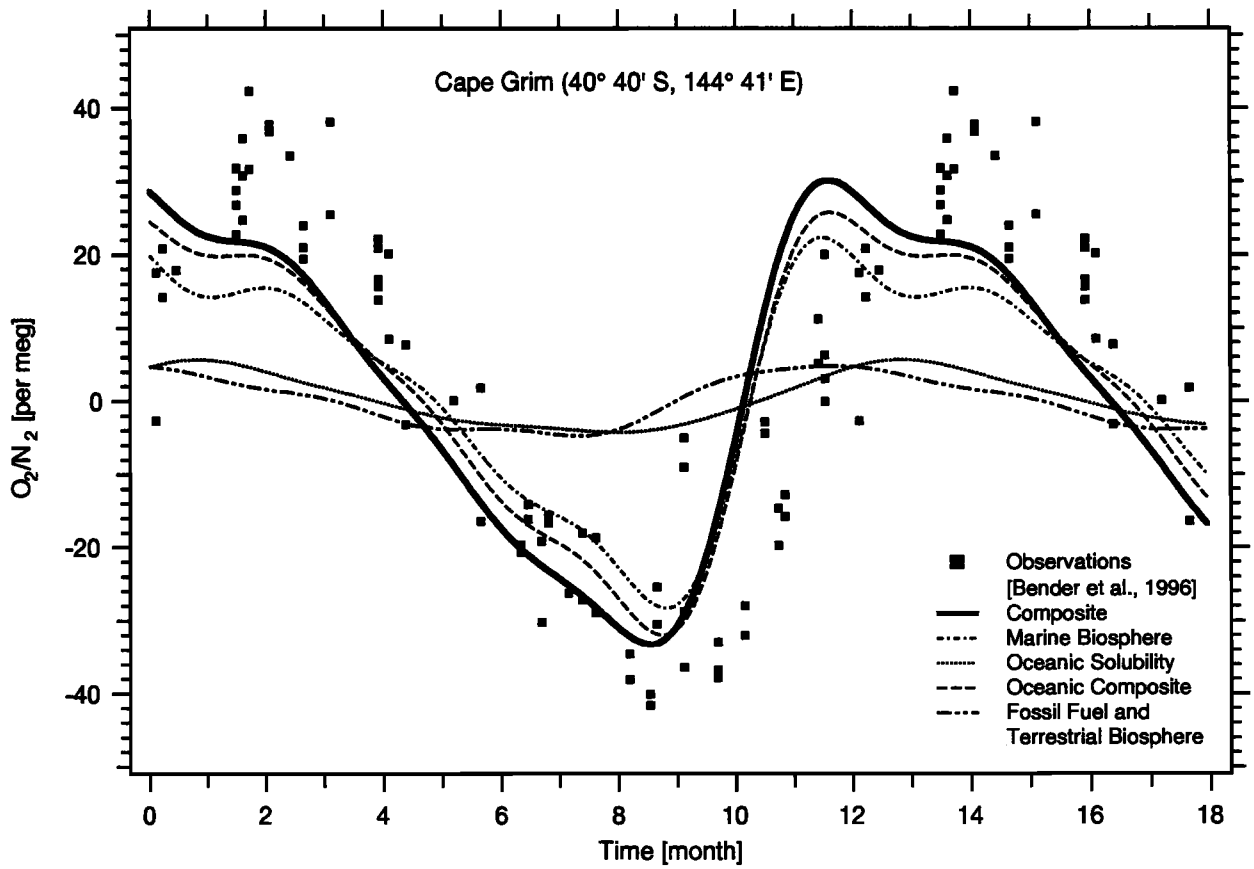

Figure 11. Seasonal variations of the relative deviations from a reference of the atmospheric oxygen to nitrogen ratio at Cape Grim, Tasmania. Units are given in per meg (1 per meg = 10^{-6}). Shown are 18 months. Squares indicate measurements from *Bender et al.* [1996].

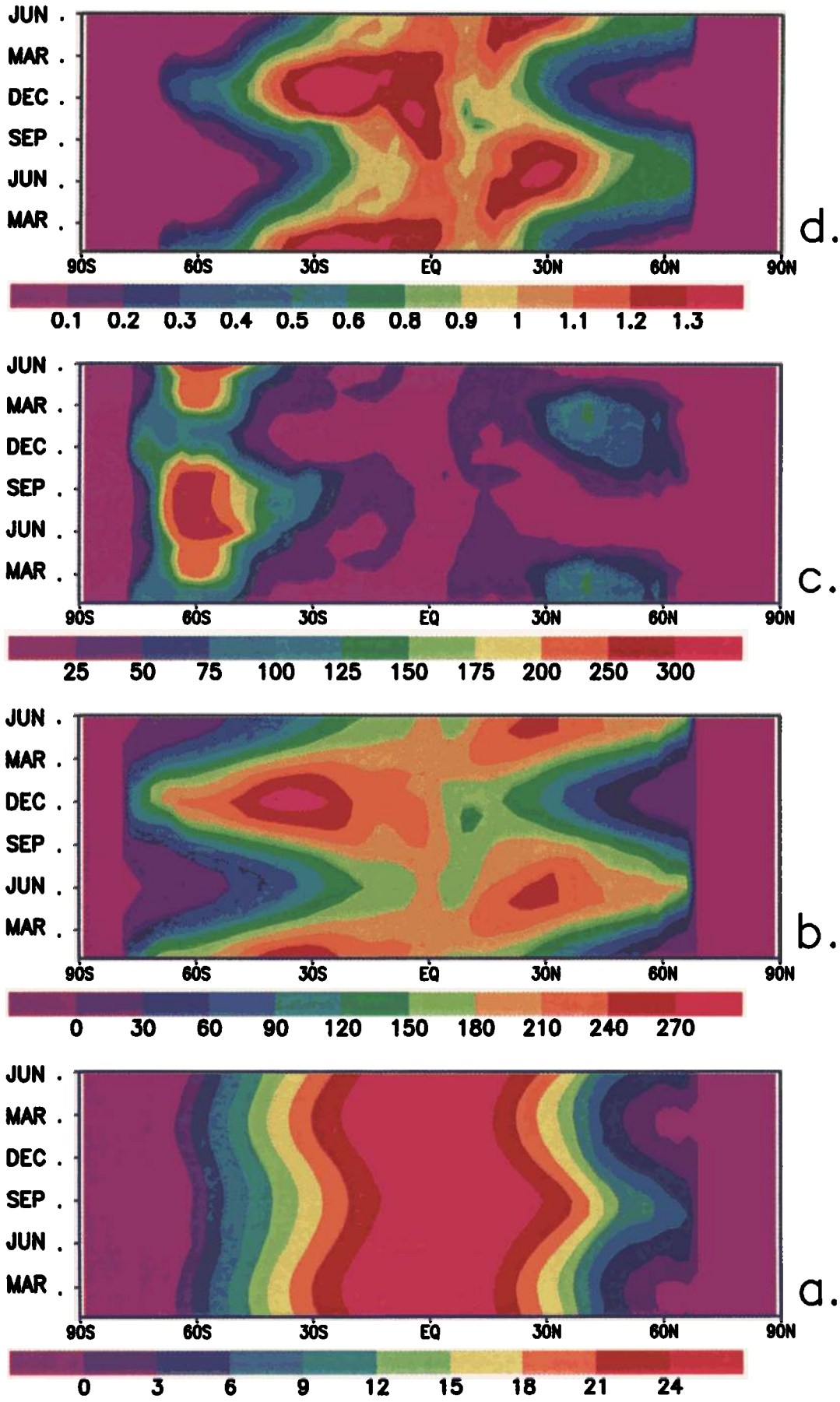

Plate 2. Time versus latitude of zonally averaged physical properties in the Pacific: (a) surface temperature (in degrees Celsius), (b) net surface irradiance (W m^{-2}), (c) simulated mixed layer depth (in meters), and (d) net growth rate of phytoplankton (per day)

one globally uniform parameterization of the biological activity dependending on the local physical environment. As far as possible, we chose the parameters in accordance with literature values. Other parameters, for example, the specific mortality rate of phytoplankton and zooplankton, were adjusted so that the simulations were consistent with observations of surface phosphate.

A good agreement with observed seasonal and regional variations in surface pCO_2 is achieved. Zooplankton dynamic causes an important part of the regional variations. The interplay between mixed layer depth, which influences the local phytoplankton growth rate, and reduced zooplankton abundance allows the development of strong phytoplankton blooms, for example, in the waters of the North Atlantic. In other regions, for example, North Pacific, relatively shallow mixed layer depths allow the support of a higher zooplankton standing stock. On any seasonal variations of phytoplankton there is an immediate response by the zooplankton stock.

Tracer distributions (ΣCO_2, PO_4, and O_2) are improved compared to HAMOCC3 [*Maier-Reimer*, 1993] because of transport of organic material within the surface layer and thus a decoupling of production and remineralization areas. This lateral transport of organic material leads to a reduction of the nutrient trapping in the Equatorial Pacific region, a prominent deficit in previous geochemical ocean models [*Najjar et al.*, 1992; *Maier-Reimer*, 1993]. The organic matter is transported mainly in form of dissolved organic carbon (DOC). DOC in the present model is mainly produced by zooplankton excretion and has a short lifetime (less than 1 year). It represents the more labile fraction of DOC. The refractory part of about 40 μmol C L^{-1} is considered as backround concentration and used only for the comparison with DOC measurements. The simulated labile fraction is confined to the upper ocean (less than 1% of the surface value in 300 m depth). The vertical DOC distribution and the seasonal DOC variations are in agreement with the very sparse measurements. The seasonal buildup of a local DOC pool allows us to simulate ΔpCO_2 variations in the vicinity of relatively low plankton concentrations. Without DOC, unrealistically high plankton concentrations were necessary to achieve consistency with the ΔpCO_2 data [*Kurz*, 1993].

The seasonal turnover of organic matter is linked to the oceanic oxygen cycle. Thus the recent atmospheric O_2/N_2 measurements [*Keeling and Shertz*, 1993; *Bender et al.*, 1996] provide a powerful constraint on the marine biological scheme. The integration of the results of oceanic and terrestrial carbon cycle models with an atmospheric transport model provides additional information about the various model components. It also gives insight into the different contributions of ocean and land biosphere to the observed atmospheric tracer variations. Ideally, one would obtain globally consistent information about the seasonal pCO_2 flux between ocean and atmosphere by simulating O_2/N_2 and $\delta^{13}C$ variations with such a combined model.

The presented model is one step toward a complete description of the ocean carbon cycle. The qualitative good agreement between model results and observations provides some confidence that the seasonal effect of marine biology is captured by the very simple plankton model. All internal structures are the results of the model parametrization and the atmospheric forcing data. This allows applications to specific climatic conditions and a full atmospheric coupling. However, tests with additional data sets and a continuous revision of the parameterized processes are undoubtedly necessary.

Acknowledgments. We thank Bob Bacastow for his help on the manuscript. We greatly appreciate the fruitful discussions with M. Bender, W. Broecker, M. Fasham, M. Heimann, C. Heinze, J. Kaduk, R. Keeling, D. Müller-Navarra, and A. Spitzy. Many thanks to M. Bender and one anonymous reviewer, who offered constructive comments to further improve the manuscript. The work has been supported by EC under Contract EV5V-CT92-0124.

References

Antia, N. J., C. D. McAllister, T. R. Parsons, K. Stephens, and J. D. H. Strickland, Further measurements of primary production using a large-volume plastic sphere, *Limnol. Oceanogr., 8*, 166-183, 1963.

Amon, R. H. W., and R. Benner, Rapid cycling of high molecular weight dissolved organic matter in the ocean, *Nature, 369*, 549-552, 1994.

Bacastow, R., and E. Maier-Reimer, Ocean-circulation model of the carbon cycle, *Clim. Dyn., 4*, 95-125, 1990.

Bacastow, R., and E. Maier-Reimer, Dissolved organic carbon in modeling oceanic new production, *Global Biogeochem. Cycles, 5*, 71-85, 1991.

Bainbridge, A. E., *GEOSECS Atlantic Expedition, Hydrographic Data*, vol. 2, Natl. Sci. Found., Washington, D. C., 1980.

Bainbridge, A. E., *GEOSECS Pacific Expedition, Hydrographic Data*, vol. 4, Natl. Sci. Found., Washington, D. C., 1981.

Banse, K., Uptake of inorganic carbon and nitrate by marine phytoplankton and the Redfield ratio, *Global Biogeochem. Cycles, 8*, 81-84, 1994.

Bender, M., T. Ellis, P. Tans, R. Francey, and D. Lowe, Variability in the O2/N2 ratio of southern hemisphere air, 1991-1994: Implications for the carbon cycle, *Global Biogeochem. Cycles, 10*, 9-21, 1996.

Berger, W. H., K. Fischer, C. Lai, and G. Wu, Ocean productivity and organic carbon flux, I, Overview and maps of primary production and export production, *SIO Ref. 87-30*, Scripps Inst. of Oceanogr., La Jolla, Calif., 1987.

Bodungen, B. v., and P. Kähler, Dissolved organic carbon in the Atlantic Ocean - Regional and seasonal patterns, *Eos, Trans. AGU, 75*(3), Ocean Sci. Meet. Suppl., 106, 1994.

Broecker, W. S., Keeping global change honest, *Global Biogeochem. Cycles, 5*, 191-192, 1991.

Broecker, W. S., T.-H. Peng, G. Östlund, and M. Stuiver, The distribution of bomb radiocarbon in the ocean, *J. Geophys. Res., 90*, 6953-6970, 1985.

Carlson, C. A., H. W. Ducklow, and A. F. Michaels, Annual flux of dissovled organic carbon from the euphotic zone in the northwestern Sargasso Sea, *Nature, 371*, 405-408, 1994.

Chipman, D. W., J. Marra, and T. Takahashi, Primary production at 47°N and 20°W in the North Atlantic Ocean: A comparison between the ^{14}C incubation method and the mixed layer carbon budget, *Deep Sea Res., Part II, 40*, 151-169, 1993.

Codispoti L. A. and J. P. Christensen, Nitrification, denitrification and nitrous oxide cycling in the eastern tropical South Pacific Ocean, *Mar. Chem., 16*, 277-300, 1985.

Conkright, M. E., S. Levitus, and T. P. Boyer, NOAA Atlas NESDIS 1: World ocean atlas 1994, vol. 1, Nutrients, technical report, 150 pp., Natl. Oceanic and Atmos. Admin., Silver Spring, Md., 1994.

Copin-Montégut, G., and B. Avril, Vertical distribution and temporal variation of dissolved organic carbon in the northwestern Mediterranean Sea, *Deep Sea Res., 40* 1963-1972, 1993.

Degens, E. T., S. Kempe, and A. Spitzy, Carbon dioxide: A biogeochemical portrait, in *The Handbook of Environmental Chemistry*, vol. 1, part C, edited by O. Hutzinger, pp. 127-215, Springer-Verlag, New York, 1984.

Devol, A. H., Direct measurements of nitrogen gas flux from continental shelf sediments, *Nature, 349*, 319-321, 1991.

Dugdale, R. C., and J. J. Goering, Uptake of new and regenerated forms of nitrogen in primary production, *Limnol. Oceanogr., 12*, 196-206, 1967.

Edmond, J. M., and J. M. T. M. Gieskes, On the calculation of the degree of saturation of sea water with respect to calcium carbonate under in situ conditions, *Geochim. Cosmochim. Acta, 34*, 1261-1291, 1970.

Eppley, R. W., Temperature and phytoplankton growth in the sea, *Fish. Bull., 70*, 1063-1085, 1972.

Eppley, R. W., and B. J. Peterson, Particulate organic matter flux and planktonic new production in the deep ocean, *Nature, 282*, 677-680, 1979.

Eppley, R. W., J. N. Rogers, and J. J. McCarthy, Halfsaturation constants for uptake of nitrate and ammonium by marine phytoplankton, *Limnol. Oceanogr., 14*, 912-920, 1969.

Evans, T. G., and J. S. Parslow, A model of annual plankton cycles, *Biol. Oceanogr., 3*, 327-347, 1985.

Fasham, M. J. R., J. L. Sarmiento, R. D. Slater, H. W. Ducklow, and R. Williams, Ecosystem behavior at Bermuda Station "S" and Ocean Weather Station "India": A general circulation model and observational analysis, *Global Biogeochem. Cycles, 7*, 379-416, 1993.

Feldman, G. C., et al., Ocean color: Availability of the global dat set, *Eos Trans. AGU, 70*(23), 634-635, 640-641, 1989.

Frost, B. W., Grazing control of phytoplankton stock in the open subarctic Pacific Ocean: A model assessing the role of mesozooplankton, particularly the large calanoid copepodes Neocalanus spp., *Mar. Ecol. Prog. Ser., 39*, 49-68, 1987.

Frost, B. W., The role of grazing in nutrient-rich areas of the open sea, *Limnol. Oceanogr., 36*, 1616-1630, 1991.

Gordon, H. R., D. K. Clark, J. W. Brown, O. B. Brown, and R. H. Evans, Satellite measurements of the phytoplankton pigment concentration in the surface waters of a warm core Gulf Stream ring, *J. Mar. Res., 40*, 491-502, 1982.

Goyet, C., and A. Poisson, New determination of carbonic acid dissociation constants in seawater as a function of temperature and salinity, *Deep Sea Res., 36*, 1635-1654, 1989.

Heimann, M., and C. D. Keeling, A three-dimensional model of atmospheric CO_2 transport based on observed winds, 2, Model description and simulated tracer experiments, in *Aspects of Climate Variability in the Pacific and the Western Americas, Geophys. Monogr. Ser.*, vol. 55, edited by D. H. Peterson, pp. 237-276, AGU, Washington D. C., 1989.

Heimann, M., and P. Monfray, Spatial and temporal variation of the gas exchange coefficient for CO_2, 1, Data analysis and global validation, *MPI Rep. 31*, Max-Planck-Inst. für Meteorol., Hamburg, Germany, 1989.

Hellermann, S., and M. Rosenstein, Normal monthly windstress over the world ocean with error estimates, *J. Phys. Oceanogr., 24*, 619-637, 1983.

Jassby, A. D., and T. Platt, Mathematical formulation of the relationship between photosynthesis and light for phytoplankton, *Limnol. Oceanogr., 21*, 540-547, 1976.

Keeling, R. F., and S. R. Shertz, Seasonal and interannual variations in atmospheric oxygen and implications for the global carbon cycle, *Nature, 358*, 723-727, 1992.

Kirchman, D. L., Y. Suzuki, C. Garside, and H. W. Ducklow, High turnover rates of dissolved organic carbon during a spring phytoplankton bloom, *Nature, 352*, 512-614, 1991.

Knorr, W., and M. Heimann, Impact of drought stress and other factors on seasonal land biosphere CO_2 exchange studied through an atmospheric tracer model, *Tellus, Ser. B, 47*, 471-489, 1995.

Kurz, K. D., Zur saisonalen Variation des ozeanischen Kohlendioxidpartialdruckes, *Examensarb. 18*, Max-Planck-Inst. für Meteorol., Hamburg, Germany, 1993.

Lampert, W., and U. Sommer, *Limnoökologie*, 440 pp., Thieme, Stuttgart, Germany, 1993.

Levitus, S., and T. P. Boyer, NOAA Atlas NESDIS 2: World ocean atlas 1994, Vol. 2, Oxygen, technical report, 186 pp., Natl. Oceanic and Atmos. Admin., Silver Spring, Md., 1994.

Lindley, S. T., R. R. Bidigare, and R.T. Barber, Phytoplankton photosynthesis parameters along 140°W in the equtaorial Pacific, *Deep Sea Res., Part II, 42*, 441-463, 1995.

Liss, P. S., and L. Merlivat, Air-sea gas exchange rates: Introduction and synthesis, in *The Role of Air-Sea Exchange in Geochemical Cycling*, edited by P. Buat-Ménard, pp. 113-127, D. Reidel, Norwell, Mass., 1986.

Maier-Reimer, E., Geochemical cycles in an ocean general circulation model: Preindustrial tracer distributions, *Global Biogeochem. Cycles, 7*, 3, 645-677, 1993.

Maier-Reimer, E., CFC Simulations, *ATOC Occas. Notes 18*, Scripps Inst. of Oceanogr., La Jolla, Calif., 1994.

Maier-Reimer, E., and R. Bacastow, Modelling of geochemical tracers in the ocean, in *Climate-Ocean Interaction*, edited by M. E. Schlesinger, vol. *NATO ASI Ser., C243*, 233-267, 1990.

Maier-Reimer, E., and K. Hasselmann, Transport and storage of CO_2 in the ocean - An inorganic ocean-circulation carbon cycle model, *Clim. Dyn. 2*, 63-90, 1987.

Maier-Reimer, E., U. Mikolajewicz, and K. Hasselmann, Mean circulation of the Hamburg LSG OGCM and its sensitivity to the thermohaline surface forcing, *J. Phys. Oceanogr., 23*, 731-757, 1993.

Maier-Reimer, E., U. Mikolajewicz, and A. Winguth, Future ocean uptake of CO_2: Interaction between ocean circulation and biology, *Clim. Dyn., 12*, 711-721, 1996.

Martin, J. H., G. A. Knauer, D. M. Karl, and W. W. Broenkow, VERTEX: Carbon cycling in the northeast Pacific, *Deep Sea Res., 34*, 267-285, 1987.

Martin, J. H., R. M. Gordon, and S. E. Fitzwater, Iron in Antarctic waters, *Nature, 345*, 156-158, 1990.

Murray, J. W., R. T. Barber, M. R. Roman, M. P. Bacon, and R. A. Feely, Physical and biological controls on carbon cycling in the equatorial Pacific, *Science, 266*, 58-65, 1994.

Najjar, R. G., J. L. Sarmiento, and J. R. Toggweiler, Downward transport and fate of organic matter in the ocean: Simulations with a general circulation model, *Global Biogeochem. Cycles, 6*, 45-76 , 1992.

Parsons, T. R., M. Takahashi, and B. Hargrave, *Biological Oceanographic Processes*, 330 pp., Pergamon, Tarrytown, N. Y., 1984.

Ramonet, M., Variabilité du CO_2 atmospherique en régions australes: Comparaison modèle/mesures, Ph.D. thesis, Univ. of Paris 7, Paris, 1994.

Raymont, J. E. G.(Ed.), *Plankton and Productivity in the Oceans*, vol. 2, 824 pp., Pergamon, Tarrytown, N. Y., 1983.

Redfield, A. C., B. H. Ketchum, and F. A. Richards, The influence of organisms on the composition of sea-water, in *The Sea*, vol. 2, edited by M. N. Hill,pp. 26-77, Wiley-Interscience, New York, 1963.

Sarmiento, J. L., J. C. Orr, and U. Siegenthaler, A perturbation simulation of CO_2 uptake in an ocean general circulation model, *J. Geophys. Res., 97*, 3621-3645, 1992.

Sarmiento, J. L., R. D. Slater, M. J. R. Fasham, H. W. Ducklow, J. R. Toggweiler, and G. T. Evans, A seasonal three-dimensional ecosystem model of nitrogen cycling in the North Atlantic euphotic zone, *Global Biogeochem. Cycles, 7*, 417-450, 1993.

Smith, E. L., Photosynthesis in relation to light and carbon dioxide, *Proc. Natl. Acad. Sci. U.S.A., 22*, 504-511, 1936.

Suess, E., Particulate organic carbon flux in the oceans - Surface productivity and oxygen utilization, *Nature, 288*, 260-263, 1980.

Sugimura, Y., and Y. Suzuki, A high-temperature catalytic oxidation method for the detemination of non-volatile dissolved organic carbon in seawater by direct injection of a liquid sample, *Mar. Chem., 24*, 105-131, 1988.

Sullivan, C. W., K. R. Arrigo, C. R. McClain, J. C. Comiso, and J. Firestone, Distributions of phytoplankton blooms in the Southern Ocean, *Science, 262*, 1832-1837, 1993.

Suzuki, Y. On the measurement of DOC and DON in seawater, *Mar. Chem., 41*, 287-288, 1993.

Sverdrup, H. U., On conditions for the vernal blooming of phytoplankton, *J. Cons. Cons. Int. Explor. Mer, 18*, 287-295, 1953.

Takahashi, T., W. S. Broecker, and S. Langer, Redfield ratio based on chemical data from isopycnal surfaces, *J. Geophs. Res., 90*, 6907-6924, 1985.

Takahashi, T., J. Olafsson, J. G. Goddard, D. W. Chipman, and S. C. Sutherland, Seasonal variation of CO_2 and nutrients in the high-latitude surface ocean: A comparative study, *Global Biogeochem. Cycles, 7*, 843-878, 1993.

Toggweiler, J. R. and S. Carson, What are upwelling systems controbuting to the ocean's carbon and nutrient budgets? in *Upweeling in the Ocean: Modern Processes and Ancient Records*, edited by C. P. Summerhayes, K.-C. Emeis, M. V. Angel, R. L. Smith, and B. Zeitzschel, pp. 337-360, John Wiley & Sons, New York, 1995.

Watson, A. J., C. Robinson, J. E. Robinson, P. J. le B. Williams, and M. J. R. Fasham, Spatial variability in the sink for atmospheric carbon dioxide in the North Atlantic, *Nature, 350*, 50-53, 1991.

Weiss, R. F., Carbon dioxide in water and seawater: The solubility of a non-ideal gas, *Mar. Chem., 2*, 203-215, 1974.

Wong, C. S., and Y.-H. Chan, Temporal variations in the partial pressure and flux of CO_2 at station P in the subarctic northeast Pacific Ocean, *Tellus, Ser. B, 43*, 206-223, 1991.

Yoder, J. A., C. R. McClain, G. C. Feldman, and W.E. Esaias, Annual cycles of phytoplankton chlorophyll concentrations in the global ocean: A satellite view, *Global Biogeochem. Cycles, 7*, 181-193, 1993.

E. Maier-Reimer and K. D. Six, Max-Planck-Institut für Meteorologie, Bundesstraße 55, D-20146 Hamburg, Germany. (e-mail: maier-reimer@dkrz.de; six@dkrz.de)

(Received January 2, 1996; revised June 18, 1996; accepted July 23, 1996.)